Chapter 3

RESULTS

The complexes of $Ru(L)_2Cl_2$ (L = dmsazpy and desazpy) were prepared by reactions of $Ru(DMSO)_4Cl_2$ with 2-(*N,N*-dimethylphenylazo)thiazole (dmsazpy) or 2-(*N,N*-diethylphenylazo)thiazole (desazpy) in $CHCl_3$. They were characterized by mass spectrometry (ES-MS) , ^{1}H NMR, UV-Visible and IR spectroscopy. In addition, electrochemistry of these complexes was studied on cyclic voltammetric technique. The results were reported in this chapter.

3.1 Synthesis and characterization of dmsazpy and desazpy Ligands

3.1.1 Synthesis of dmsazpy and desazpy ligands

2-(*N,N*-dimethylphenylazo)thiazole (dmsazpy) and 2-(*N,N*-diethylphenyl azo)thiazole (desazpy) ligangs were synthesized by the coupling of thiazolylazonium ion with *N,N*-dimethylaniline and *N,N*-diethylaniline, respectively in the presence of acidic solution at low temperature. The crude product was purified by column chromatography and the reactions were followed by equation (1) and (2).

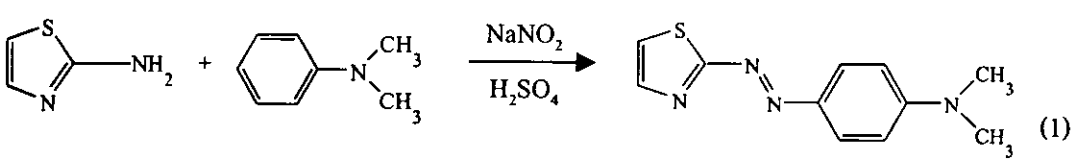

(1)

2-aminothiazole *N,N*-dimethylaniline 2-(*N,N*-dimethylphenylazo)thiazole (dmsazpy)

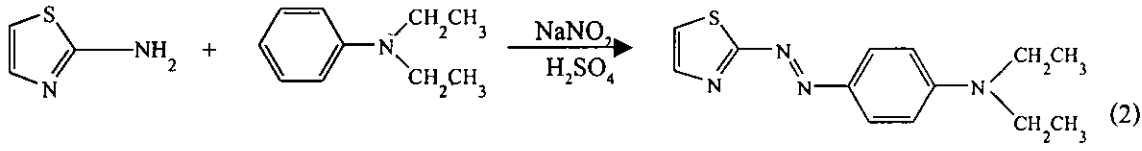

(2)

2-aminothiazole *N,N*-diethylaniline 2-(*N,N*-diethylphenylazo)thiazole (desazpy)

Dmsazpy and desazpy are unsymmetric bidentate ligands and use N(thiazole); N(th) and N(azo) as donor atoms to metal center. The synthesized ligands have red color. The yields of dmsazpy and desazpy are 50.8% and 51.6%, respectively. The solubility of dmsazpy and desazpy were summarized in Table 1.

Table 1 The solubility of dmsazpy and desazpy ligands

solvents	solubility
Hexane	+++
Toluene	+++
Dichloromethane	+++
Chloroform	+++
Ethyl acetate	+++
Acetone	+++
Acetonitrile	+++
Dimethylformamide	+++
Dimethyl sulfoxide	+++
Ethanol	+++
Methanol	+++
*water	++
*0.1 M HCl	++
*0.1 M NH_4OH	+

+ partially soluble ++ more soluble +++ well soluble *changed color

0.0012 g. of ligands, dmsazpy and desazpy were tested their solubility in 10 mL of various solvents. The symbol of solubility, + represents the partially solubility of ligands less than 0.005 g. and ++ represents the increase of solubility of ligands in the range 0.005-0.008 g. The +++ represents 0.0012 g. of those ligands completely soluble in 10 mL of solvents.

Those ligands are instantly well soluble in non-solvents and less soluble in polar solvents. However, the red ligands have immediately changed color into deep pink when they dissolved in acid due to protonation at N atoms (Klotz and Ming, 1953).

3.1.2 Characterization of dmsazpy and desazpy ligands

The structures of dmsazpy and desazpy ligands were investigated by using these techniques

3.1.2.1 Elemental analysis

3.1.2.2 Electrospray mass spectrometry

3.1.2.3 Infrared spectroscopy

3.1.2.4 Proton Nuclear Magnetic Resonance spectroscopy

3.1.2.5 UV-Visible absorption spectroscopy

3.1.2.1 Elemental analysis

Elemental analysis is the principle method to study composition of elements in the ligands. Therefore, the elements in the ligands are confirmed by this method.

Table 2 Elemental analysis data of dmsazpy and desazpy ligands

Ligands	% C		% N		% H	
	Calc.	Found.	Calc.	Found.	Calc.	Found.
dmsazpy	56.87	57.03	24.12	22.51	5.21	5.60
desazpy	59.97	60.19	21.52	20.34	6.20	6.52

3.1.2.2 Electrospray mass spectrometric data of dmsazpy and desazpy ligands

The results from electrospray mass spectroscopic data of dmsazpy and desazpy ligands are displayed in Table 3 and 4, respectively. The maximum peaks in an isotropic mass distribution are very closed to molecular weight of ligands. Therefore, it can confirm the molecular structures of ligands. The electrospray mass spectra for dmsazpy and desazpy are shown in Figure 3 and 4, respectively.

Table 3 Electrospray mass spectroscopic data of dmsazpy ligand

m/z	Fragments	Equivalent species	Rel. abun.
232.9	$[dmsazpy + H]^+$	$[M+H]^+$	100
147.9	$[(CH_3)_2NC_6H_4N{=}N]^+$	-	75
234.0	$[dmsazpy + 2H]^+$	$[M+2H]^+$	65

MW. of dmsazpy = 232.3 = M

Table 4 Electrospray mass spectroscopic data of desazpy ligand

m/z	Fragments	Equivalent species	Rel. abun.
261.1	$[desazpy + H]^+$	$[M+H]^+$	89
175.9	$[(C_2H_5)_2NC_6H_4N=N]^+$	-	100
262.0	$[desazpy + 2H]^+$	$[M+2H]^+$	63

MW. of desazpy = 260.3 = M

The dmsazpy and desazpy ligands are unstable at higher ion source energy. They undergo significant decomposition to give major species.

The spectrum peak of dmsazpy consist of a stable molecular ion at m/z 232.9 which one protonation. The other minor ion at m/z 147.9 is attributable to the loss of thiazole ring. The other fragmentation at m/z 234.0 shows two protonation on main structure.

In contrast to desazpy ligand, it shows a molecular ion at 261.1 and major stable molecular ion at m/z 175.9, which seems to occur according to loss of thiazole ring. The other fragmentation at m/z 262.0 exhibits two protonation on main structure.

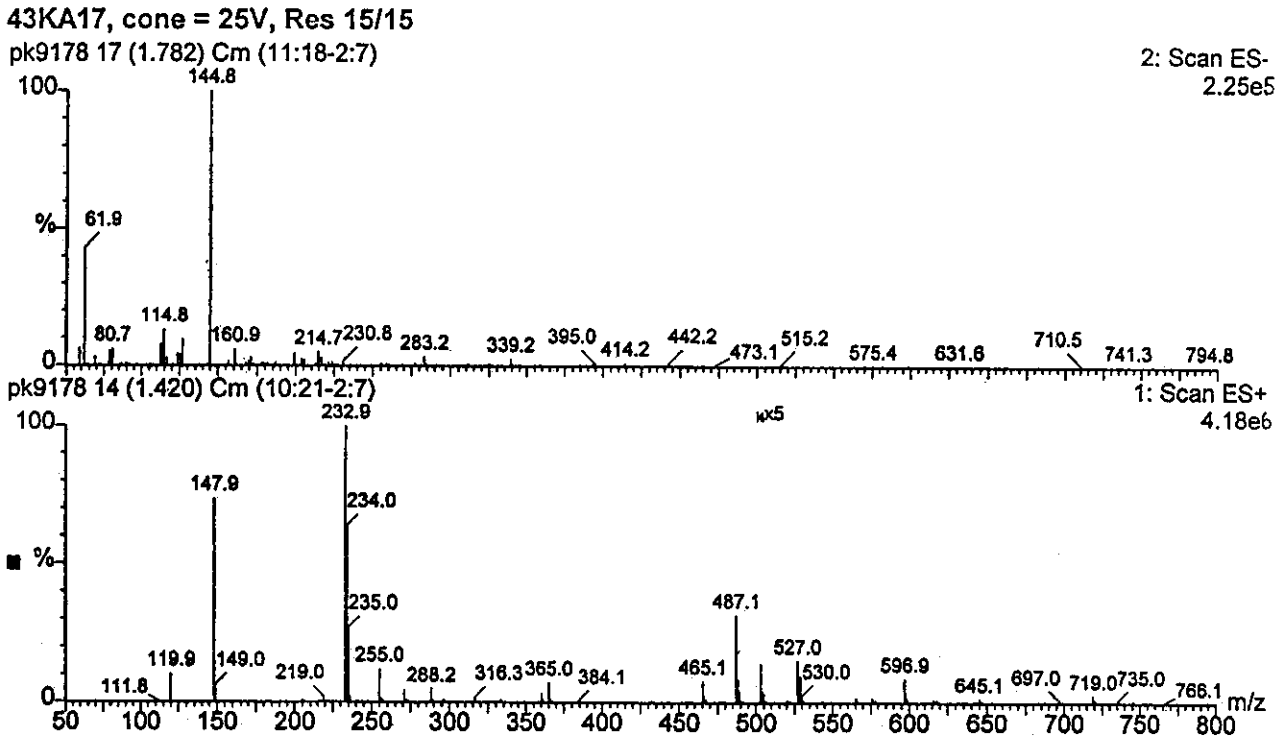

Figure 3 Electrospray mass spectrum of dmsazpy ligand

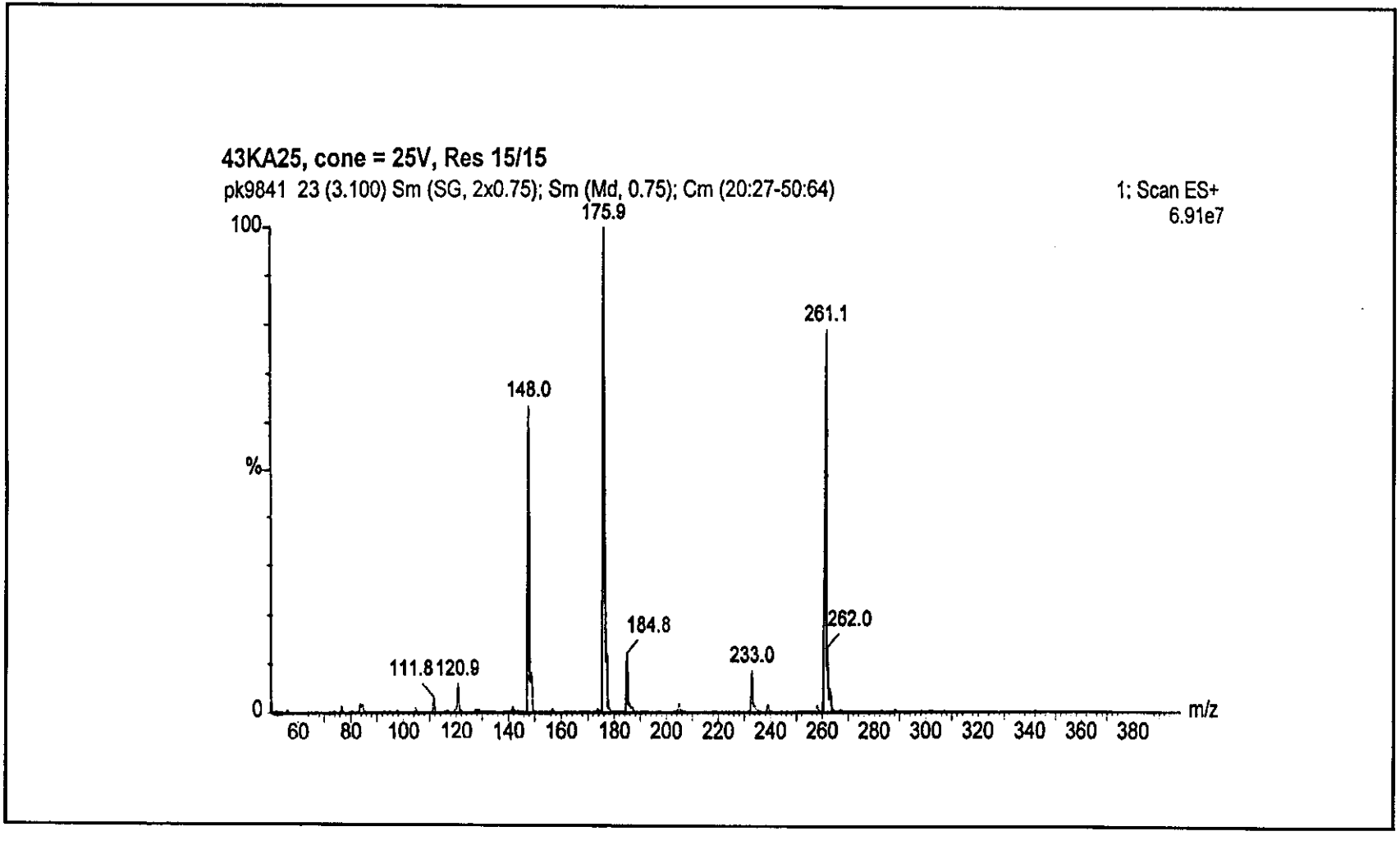

Figure 4 Electrospray mass spectrum of desazpy ligand

3.1.2.3 Infrared (IR) data of dmsazpy ligand

IR is an useful technique to identify the functional group in compounds. IR spectra of dmsazpy and desazpy ligands are recorded in the range 4000-370 cm^{-1} and shown in Figure 5 and 6, respectively. The spectra of these ligands show some characteristic frequencies in the range 1600-500 cm^{-1}. They are summarized in Table 5 and 6 for dmsazpy and desazpy, respectively.

Table 5 IR data of dmsazpy ligand

Vibration modes	Frequencies (cm^{-1})
sp^2 C-H stretching	2917(s)
N=N stretching	1367(s)
C=N stretching	1556(m)
C=C stretching	1607(s) 1556(m) 1524(m) 1422(s)
C-N stretching in aromatic amines	1366(s)
C-S-C	870(m)
C-H bending of para Disubstituted benzene	821(s)

s= strong, m= medium and w= weak

Table 6 IR data of desazpy ligand

Vibration modes	Frequencies (cm^{-1})
sp^2 C-H stretching	2969(s)
N=N stretching	1358(s)
C=N stretching	1551(s)
C=C stretching	1519(s) 1551(m) 1519(m) 1415(s)
C-N stretching in aromatic amines	863(m)
C-H bending of para Disubstituted benzene	826(s)

s= strong, m= medium and w= weak

The characteristic peaks for determining structures of dmsazpy and desazpy ligands were observed. There are several stretching modes which belong to thiazole and phenyl ring in the range 1600-800 cm^{-1} such as C=C, C=N, C-N and C-S-C. Those modes show strong to medium absorption at the frequencies similar to azpy. The C=C and C=N stretching modes of azpy appear at 1584, 1578, 1498 and 1495 cm^{-1} (Krause and Krause, 1980).

The most importance peak is N=N stretching mode which used for considering the π-acid property in azo complexes. The N=N stretching of dmsazpy and desazpy ligands show the intense peak at 1367 and 1358 cm^{-1}, respectively. Meanwhile, the N=N stretching of azpy ligand shows peak at higher frequency, 1424 cm^{-1} (Krause and Krause, 1980). The decrease of N=N bond order in dmsazpy and desazpy ligands may be due to the substituent ($-NR_2$) which are electron donating groups.

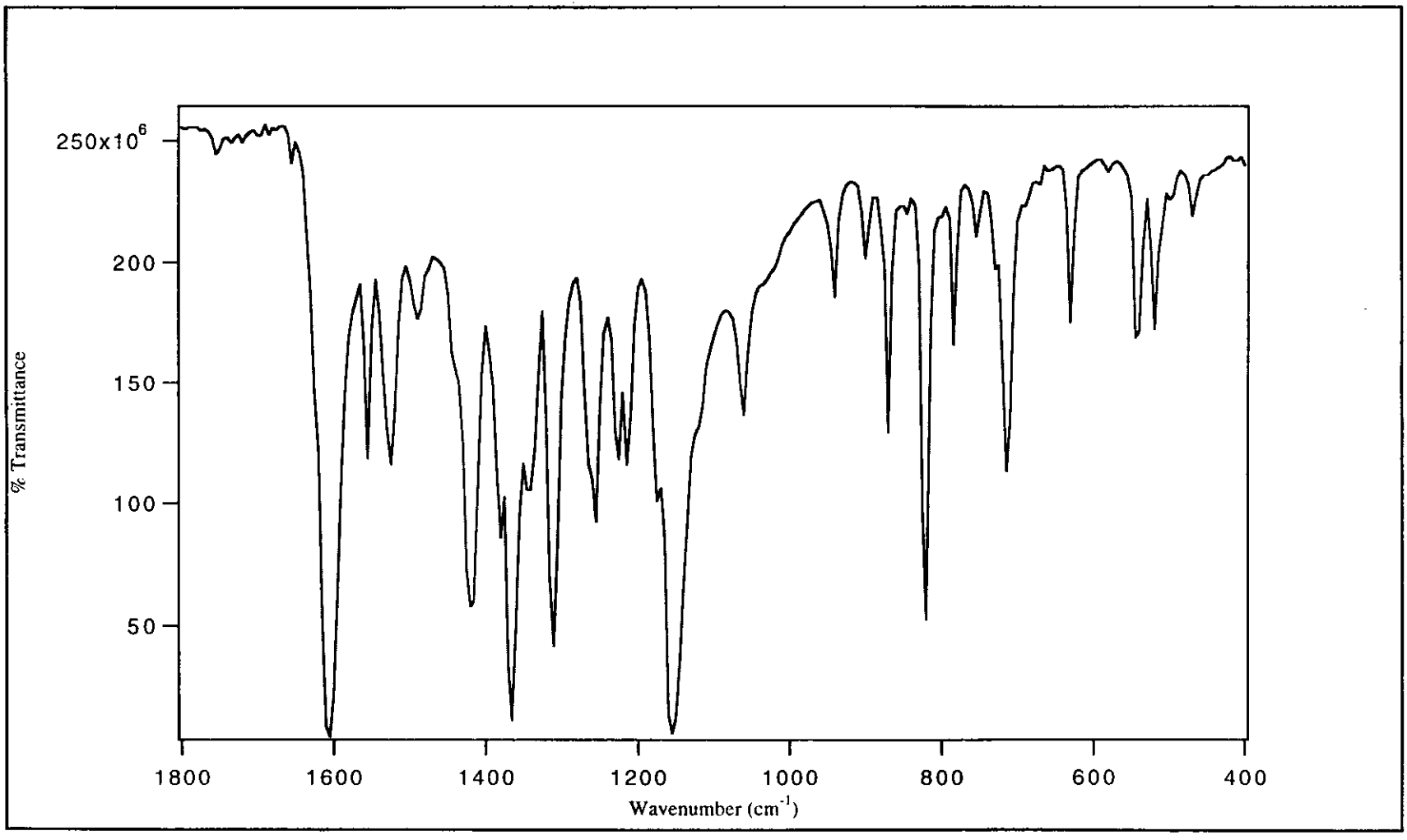

Figure 5 IR spectrum of dmsazpy ligand

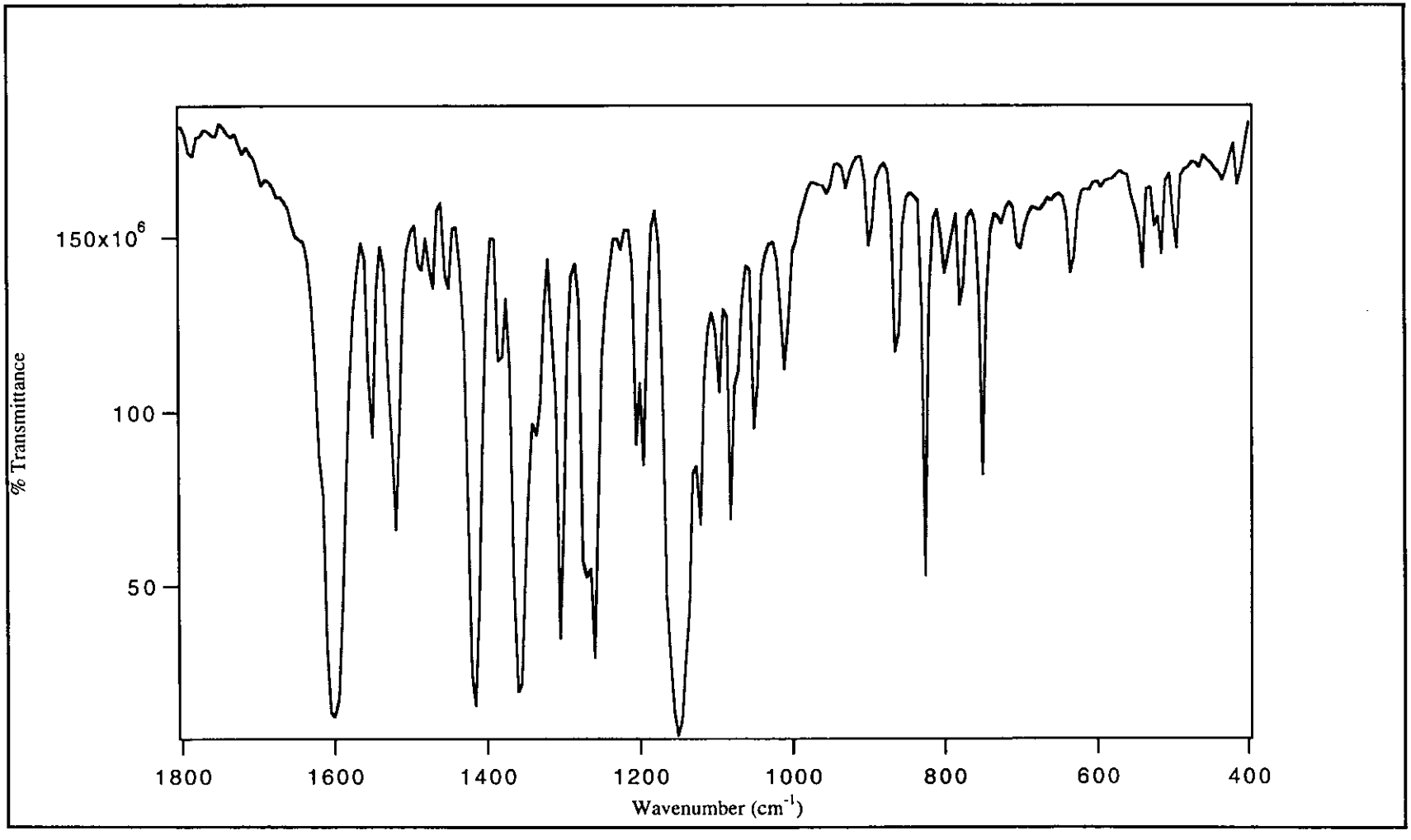

Figure 6 IR spectrum of desazpy ligand

3.1.2.4 ^{1}H NMR spectroscopic data of dmsazpy and desazpy ligands

The ^{1}H NMR spectra of dmsazpy and desazpy ligands are collected in $CDCl_3$. Tetramethylsilane (TMS, $(CH_3)_4Si$) was used as internal reference. The chemical shifts (δ, ppm) and J-coupling (Hz) of free ligands are reported in part per million (ppm) downfield from TMS. The proton numbering pattern of both ligands are shown in Figure 7. The type of protons in dmsazpy and desazpy ligands are divided into five and six groups, respectively. The spectral data are given in Table 7 for dmsazpy and Table 8 for desazpy ligands. The ^{1}H NMR spectra are displayed in Figure 8 and 9 for dmsazpy and desazpy, respectively.

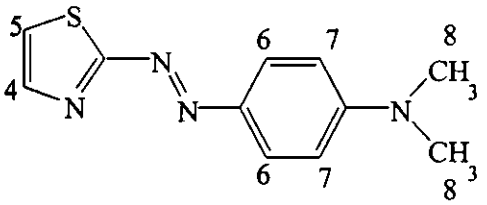

dmsazp

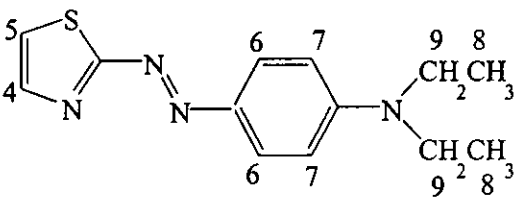

desazpy

Figure 7 Structures of dmsazpy and desazpy ligands with proton numbering systems

Table 7 ^{1}H NMR data of dmsazpy ligand

H-position	J-coupling	δ (ppm)	Amounts of H	Peak
6	9.5	7.94	2	d
4	3.5	7.90	1	d
5	3.5	7.25	1	d
7	9.0	6.73	2	d
8	-	3.12	6	s

d = doublet, s = singlet

Table 8 ^{1}H NMR data of desazpy ligand

H-position	J-coupling	δ (ppm)	Amounts of H	peak
6	9.5	7.92	2	d
4	3.0	7.89	1	d
5	3.5	7.23	1	d
7	9.5	6.72	2	d
8	7, 7.5	1.25	6	t
9	7, 7, 7	3.48	4	q

d = doublet, t = triplet, q = quartet

The ^{1}H NMR results are used to confirm molecular structure because the different protons in the molecular structure will show different chemical shifts. The ^{1}H NMR data of dmsazpy and desazpy are very similar. The detailed of each signal can be described below.

The proton-4 (H4) is on the thiazole ring next to nitrogen atom. The H4 signal is splitted by the proton-5 (J=3.5 Hz). The signal is doublet (d) peak.

The proton-5 (H5) is the proton which is between the H4 and sulfur atom. The H5 is less effected from nitrogen atom than that of the H4. Therefore, the chemical shift value is less than that the proton-4. The signal is also doublet peaks and splitted by the H4 (J=3.5-3.0 Hz).

The proton-6 (H6) which give signal at most downfield are two equivalent protons on phenyl ring located closed to azo nitrogen. The H6 interacts with H7 giving the doublet peaks with J-coupling 9.5 Hz.

The proton-7 (H7) are two equivalent protons located next to H6. The signal is also doublet peaks and splitted by the H6 (J= 9.5 Hz).

The proton-8 (H8) signal of dmsazpy are the methyl proton ($N\text{-}CH_3$). This signal is singlet of 6 protons and appears at 3.00 ppm. whereas, H8 signal of desazpy $\text{-}CH_3$ shows a triplet at 1.25 ppm and the methylene proton ($\text{-}CH_2\text{-}$), H9, shows quartet with J-coupling 7, 7.5 Hz. These chemical shifts (H8) of both ligands are the most upfield.

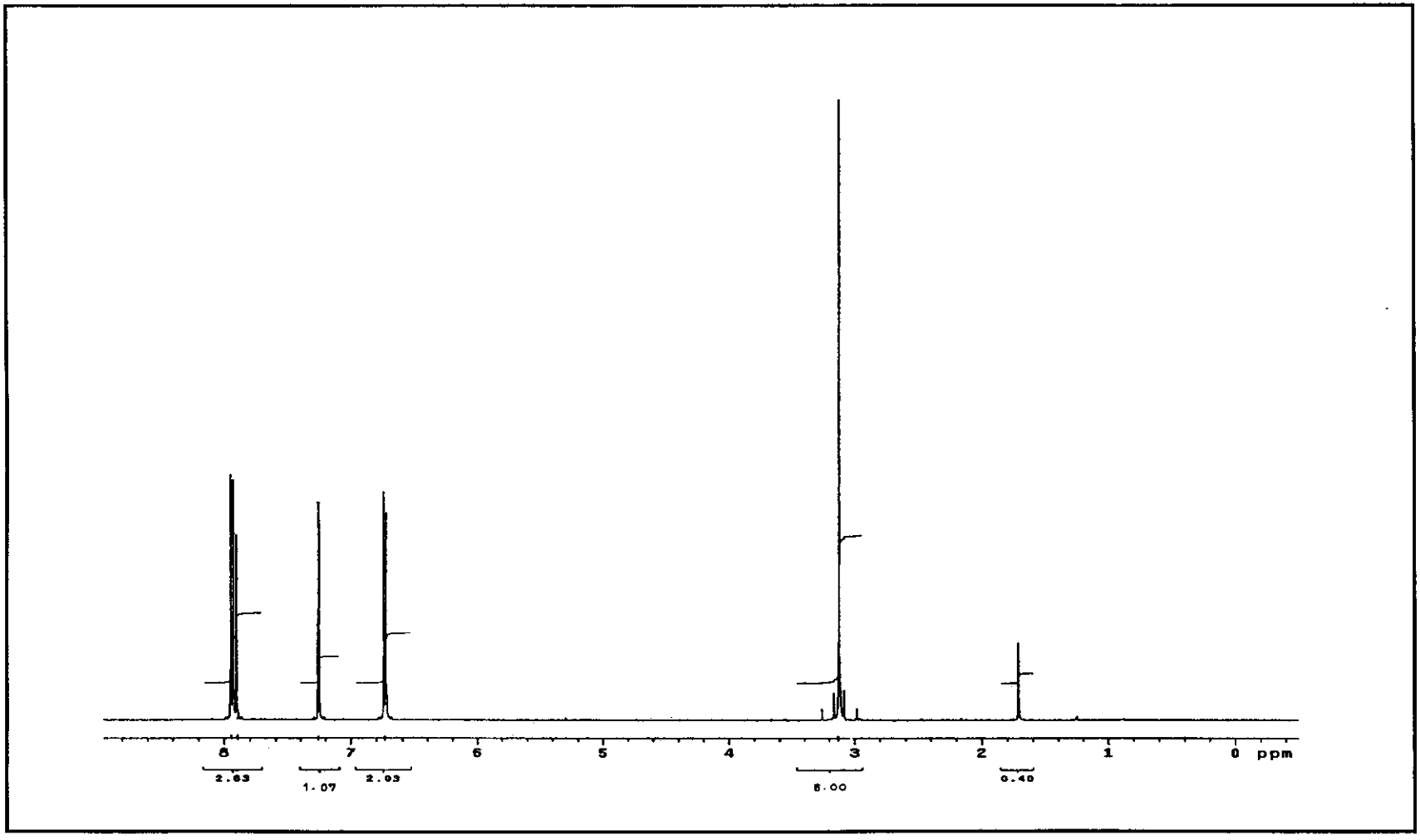

Figure 8 ^{1}H NMR spectrum of dmsazpy ligand

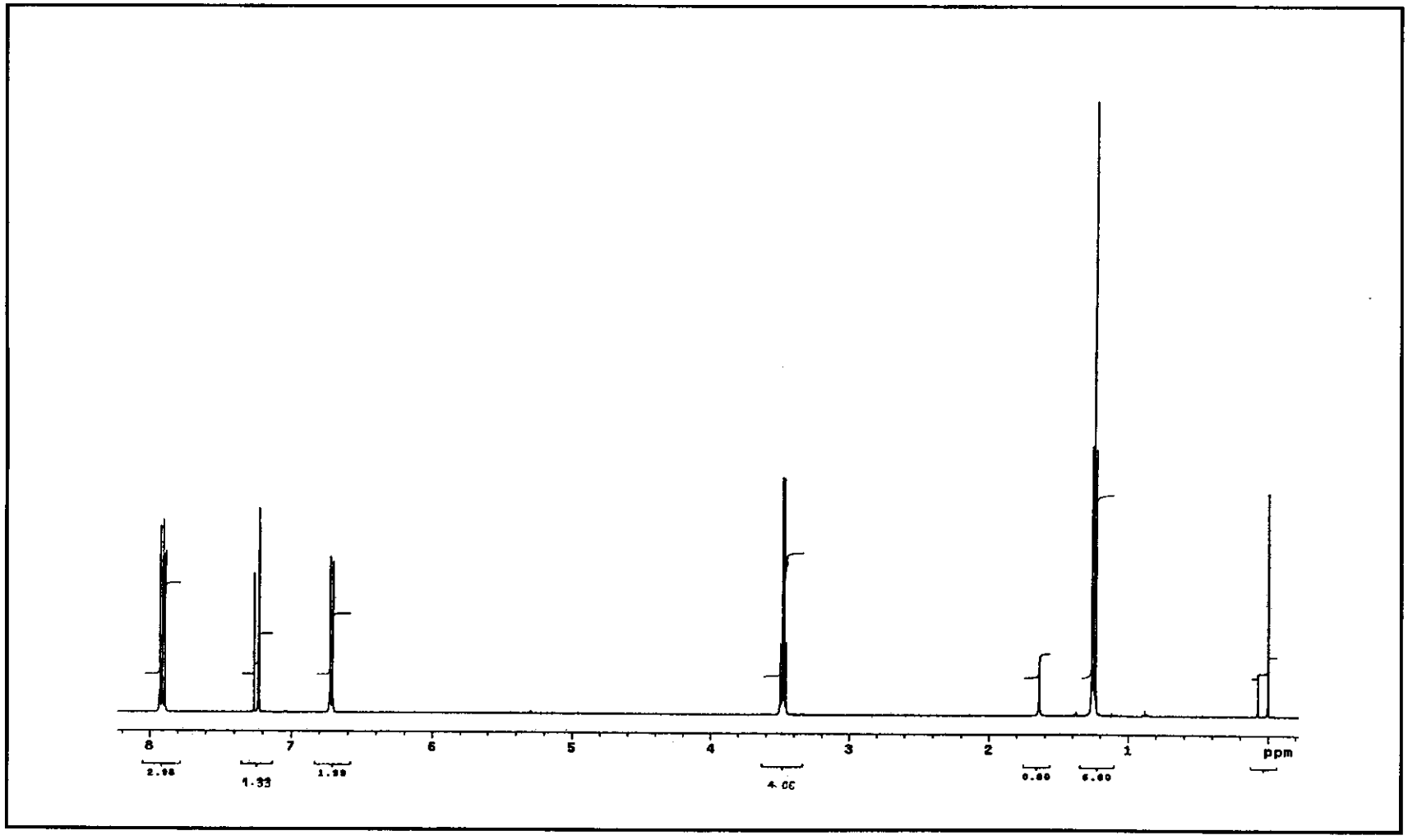

Figure 9 ^{1}H NMR spectrum of desazpy ligand

3.1.2.5 UV-Visible absorption spectroscopic data of dmsazpy and desazpy ligands

UV-Visible spectral data of both ligands exhibit absorption in the range 200-820 nm in various solvents; $CHCl_3$, CH_2Cl_2, DMF, DMSO and CH_3CN. In addition, the absorption spectra of dmsazpy and desazpy in $CHCl_3$ are shown in Figure 10 and 11, respectively. The summarized data are listed in Table 9 compared to azpy ligand.

Table 9 The UV-Vis spectral datas of azpy, dmsazpy and desazpy ligands

Compounds	Maximum Wavelength, nm (ε^a x 10^{-4}, $M^{-1}cm^{-1}$) in solvents				
	$CHCl_3$	CH_2Cl_2	DMF	DMSO	CH_3CN
azpy	320(1.18)	320(1.56)	-	320(1.96)	316(1.90)
dmsazpy	276(0.98)	278(0.78)	278(0.79)	280(0.80)	276(0.77)
	482(3.38)	486(3.77)	490(3.50)	498(3.62)	486(3.38)
desazpy	278(0.79)	280(0.95)	-	278(1.30)	278(0.80)
	490(4.00)	492(4.29)	496(3.63)	504(4.14)	490(4.35)

[a]Molar Extinction coefficient.

The azoimine ligand groups show two absorption bands in the range 300-500 nm. They are assigned to $n \rightarrow \pi^*$ and $\pi \rightarrow \pi^*$ transitions. The absorption spectrum of azpy exhibits the maximum intense band of $\pi \rightarrow \pi^*$ transition at the higher energy (320 nm., ε ~20,000$M^{-1}cm^{-1}$) and gives the weak band of $n \rightarrow \pi^*$ transition at the lower energy (~450 nm., ε ~950 $M^{-1}cm^{-1}$). Meanwhile, the dmsazpy and desazpy ligands show the absorption intense band of $\pi \rightarrow \pi^*$ transition at the lower energy

(480-504 nm., ε ~30,000-44,000 $M^{-1}cm^{-1}$). In addition, the n→ π^* transition is shifted to higher energy (~278 nm, ε ~8,000 $M^{-1}cm^{-1}$) closed to the solvent cut-off.

Furthermore, dmsazpy and desazpy ligands show slightly solvent effect. The polar solvents lead to bathochromic shift (red shift) of π→ π^* transition.

In addition, the results from spectroscopic data show that the substituents ($-NR_2$, R= CH_3, C_2H_5) on phenyl ring have influence upon the absorption spectra by shifting to lower energy.

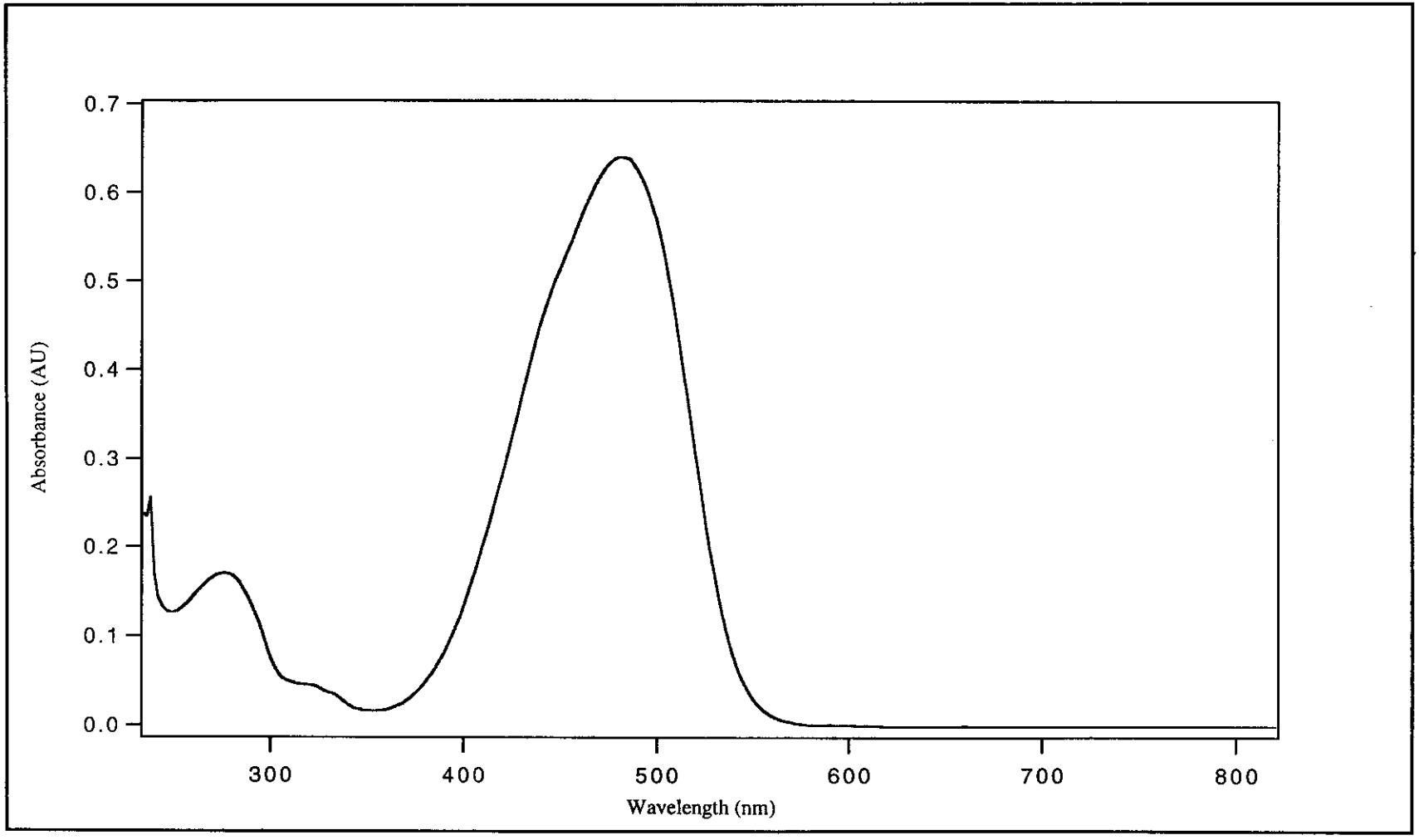

Figure 10 UV-Visible absorption spectrum of dmsazpy ligand in $CHCl_3$

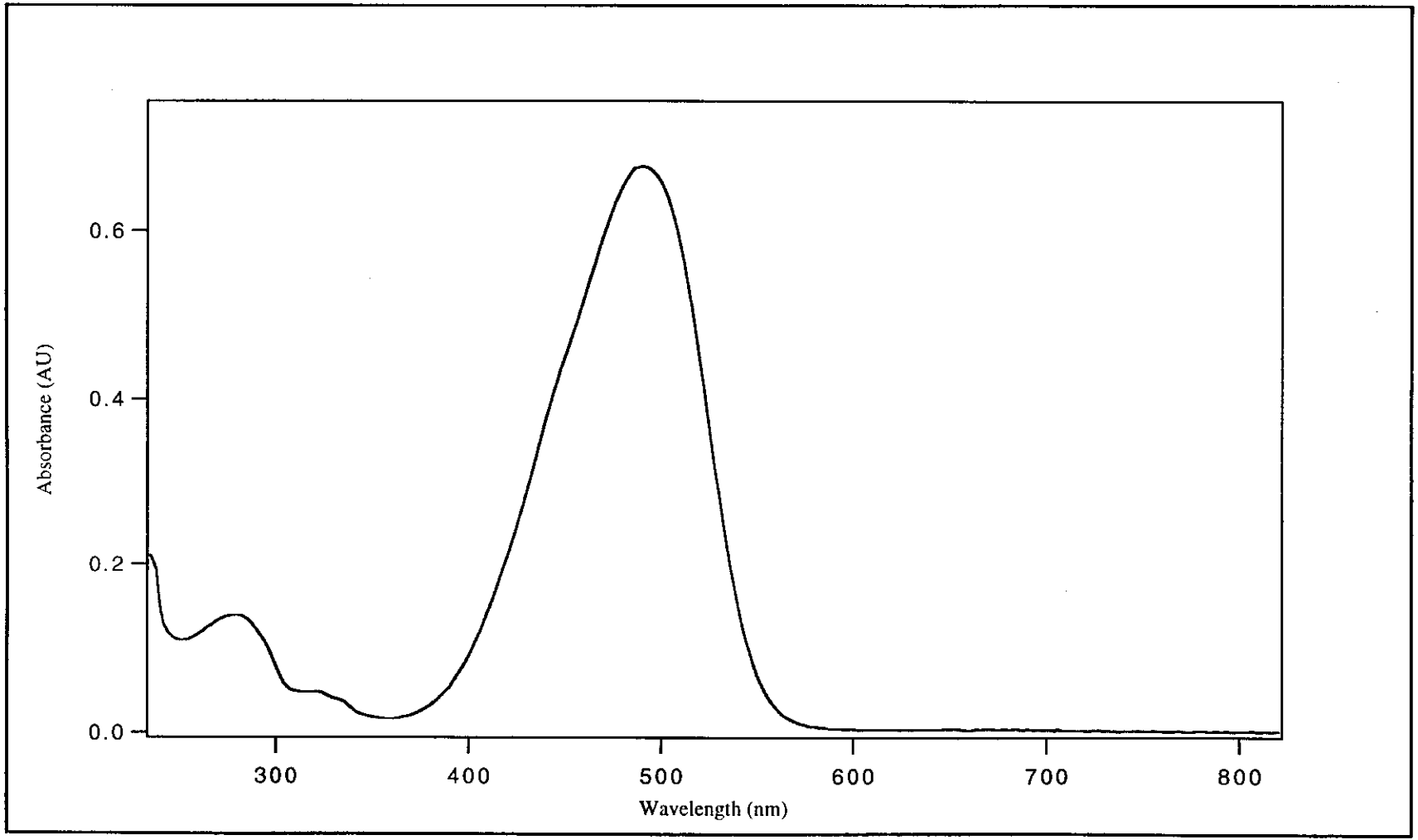

Figure 11 UV-Visible absorption spectrum of desazpy ligand in $CHCl_3$

3.2 Synthesis and characterization of $Ru(DMSO)_4Cl_2$ and $Ru(L)_2Cl_2$ (L=dmsazpy and desazpy) complexes.

3.2.1 Synthesis and characterization of $Ru(DMSO)_4Cl_2$ complex

$Ru(DMSO)_4Cl_2$ complex were synthesized and used as starting material for synthesis the complexes of $Ru(L)_2Cl_2$ (L=dmsazpy and desazpy). The $Ru(DMSO)_4Cl_2$ complex was prepared according to the literature procedure (Evans *et al.*, 1973). The structure of $Ru(DMSO)_4Cl_2$ was studied by IR spectroscopy. The results from this technique are listed in Table 10 and the IR spectra of this complex is shown in figure 12.

Table 10 IR data of $Ru(DMSO)_4Cl_2$ complex

Vibrational modes	Frequencies (cm^{-1})
sp^2 C-H stretching	3000, 2900(m)
C-H deformation	1403(m)
S-O stretching S bonded	1120, 1100(s)
C-S stretching	720(s)
Ru-S stretching	480(m)
CSO symmetric deformation	430(s)
CSO asymmetric deformation	390(m)
Ru-Cl stretching	350(m)

The IR data of the synthesized $Ru(DMSO)_4Cl_2$ complex is similar to that of Evans, *et al* (1973). A complete assignment of all bands of $Ru(DMSO)_4Cl_2$ complex shows in the range 4000-200 cm^{-1}. In general, the SO stretch in neat Me_2SO occurs at 1055 cm^{-1}, very strong and broad. If the spectra of $Ru(DMSO)_4Cl_2$ shows strong band with splitting at 1090-1120 cm^{-1}, it is assigned to SO stretching which belongs to S-bonded Me_2SO. Whereas, if the band occurs at 915 cm^{-1}, it is assigned to SO stretch of O-bonded Me_2SO (Evans, *et al.*, 1973).

In this work, the synthesized $Ru(DMSO)_4Cl_2$ complex shows only the strong band with splitting at 1100-1120 cm^{-1}. This indicates that the S atom is bonded to the ruthenium(II) center. In addition, in the range 500-400 cm^{-1}, there is the stretching band assigned belong to Ru-S which appeared at 480 cm^{-1}. Furthermore, the Ru-Cl stretching band in far IR region shows as the sharp single band at 350 cm^{-1}. It is concluded that the IR data supports the existence of S-bonded in the synthesized complex of *trans*-$Ru(DMSO)_4Cl_2$.

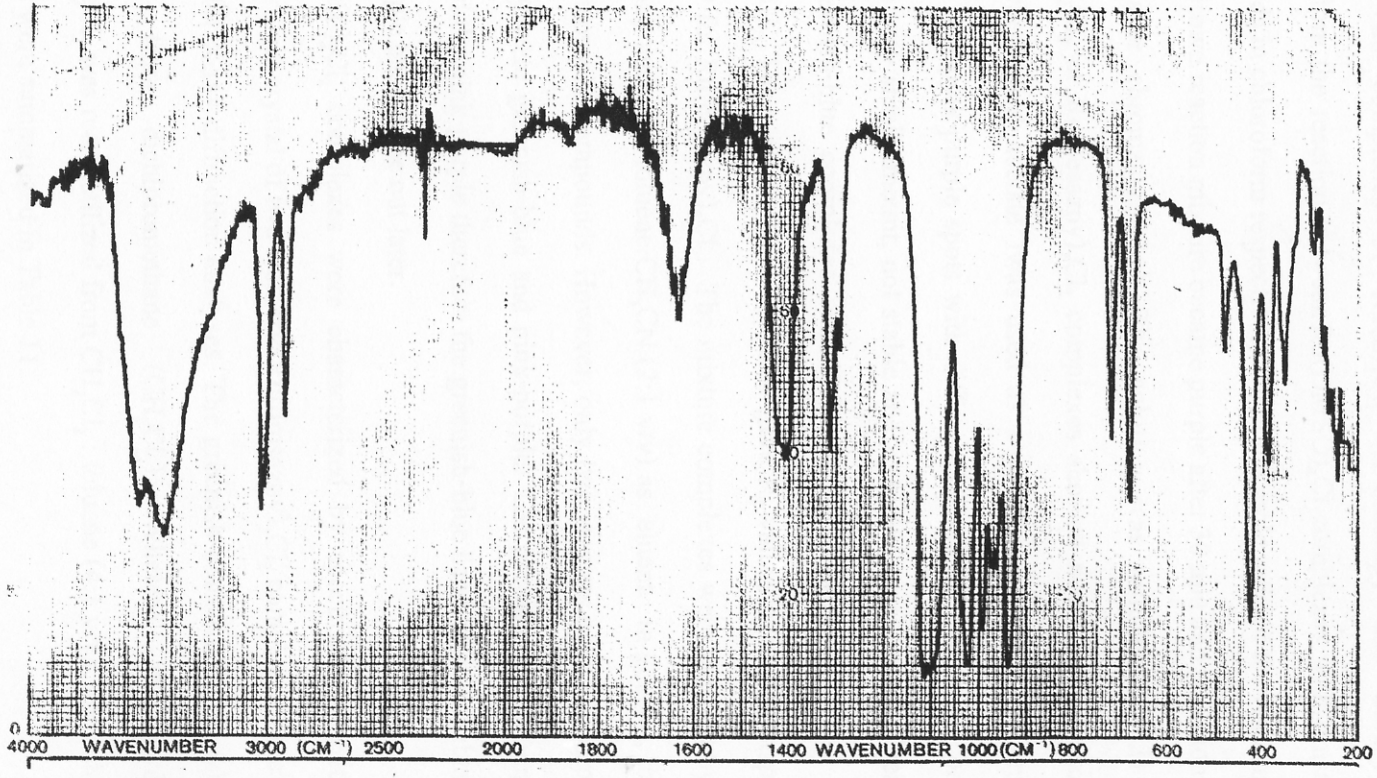

Figure 12 IR spectrum of $Ru(DMSO)_4Cl_2$ complex

3.2.2 Synthesis of $Ru(L)_2Cl_2$ (L=dmsazpy and desazpy) complexes

The complexes of $Ru(L)_2Cl_2$ (L=dmsazpy and desazpy) were synthesized from the reaction between $Ru(DMSO)_4Cl_2$complexes with dmsazpy and desazpy ligands in chloroform respectively when the mole ratio of the reactants is 1:2. The reddish-brown reaction mixture became purple after 30 min and was monitored by TLC (thin layer chromatography). The solution was refluxed for 21 h. The $Ru(dmsazpy)_2Cl_2$ or $Ru(desazpy)_2Cl_2$ complexes showed three colorful isomers on TLC plate when ethyl acetate Iwas used as a mobile solvent. They are purple, greenish-blue and pink-purple spots with different R_f values. The purple bands was collected in a very small amount, not stable and were not considered further. The R_f values of greenish-blue complexes were 0.33 for $Ru(dmsazpy)_2Cl_2$ and 0.54 for $Ru(desazpy)_2Cl_2$. The pink-purple complexes gave R_f values of $Ru(dmsazpy)_2Cl_2$ at 0.12 and 0.19 for $Ru(desazpy)_2Cl_2$. The mixture complexes were purified by column chromatography and used toluene:CH_3CN (2:1 v/v) as eluent. In general, there were five possible isomeric compounds. However, only two isomers of each complex were isolated. They were greenish-blue and pink-purple. The greenish-blue complex was less polar than the pink-purple therefore the greenish-blue band was frist obtained and the pink- purple band came out later.

The $Ru(L)_2Cl_2$ complexes were characterized by spectroscopic methods. In addition, the single crystal of two isomeric $Ru(dmsazpy)_2Cl_2$ complexes were obtained and suitable for X-ray diffraction analyses. The greenish-blue, $Ru(dmsazpy)_2Cl_2$ was recrystallized from dichloromethane (CH_2Cl_2). Whereas, the pink-purple, $Ru(dmsazpy)_2Cl_2$ was recrystallized from CH_2Cl_2 : toluene (4:1 v/v). The solubility of all complexes were summarized in Table 11.

Table 11 The solubility of *trans*-$Ru(L)_2Cl_2$ and *cis*-$Ru(L)_2Cl_2$ complexes

Solvents	Solubility of complexes	
	trans- $Ru(L)_2Cl_2$	*cis*-$Ru(L)_2Cl_2$
Hexane	-	-
Toluene	+	++
Dichloromethane	+++	+++
Chloroform	+++	+++
Ethyl acetate	+	+
Acetone	+	+
Acetonitrile	++	++
Dimethylformamide	+++	+++
Dimethyl sulfoxide	+++	+++
Methanol	+	++
Ethanol	+	++
Water	-	-
$^{\bullet}HCl$	-	-
$^{\bullet}NH_4OH$	-	-

- nonsoluble + partially soluble ++ more soluble +++ well soluble

0.0011 g. of all complexes were tested their solubility in 10 mL of various solvents. The symbol of solubility, + represents the partially solubility of those complexes less than 0.0003 g. and ++ represents the increase of solubility of complexes in the range 0.0004-0.0009 g. The +++ represents 0.0011 g. of complexes completely soluble in 10 mL of solvents.

The solubility of complexes is useful for recrystallization. The suitable solvents may be selected from solvent in which complexes have different solubility.

3.2.3 Characterization of $Ru(L)_2Cl_2$ (L=dmsazpy and desazpy) complexes

The complexes of $Ru(L)_2Cl_2$ (L=dmsazpy and desazpy) were synthesized and characterized by using these following techniques.

3.2.3.1 Elemental analysis

3.2.3.2 Electrospray mass spectrometry

3.2.3.3 Infrared spectroscopy

3.2.3.4 Proton Nuclear Magnetic Resonance spectroscopy

3.2.3.5 UV-Visible absorption spectroscopy

3.2.3.1 Elemental analysis

Elemental analysis is the principle method to composition of elements in the complexes. Therefore, the elements in the complexes are confirmed by this method.

Table 12 Elemental analysis data of *trans*- and *cis*-$Ru(L)_2Cl_2$ (L = dmsazpy and desazpy) complexes

Complexes	% C		% N		% H	
	Calc.	Found.	Calc.	Found.	Calc.	Found.
trans-$Ru(dmsazpy)_2Cl_2$	41.51	41.53	17.60	16.44	3.80	4.09
trans-$Ru(desazpy)_2Cl_2$	45.08	45.57	16.18	15.00	4.66	5.06
cis-$Ru(dmsazpy)_2Cl_2$	41.51	41.37	17.60	16.42	3.80	4.00
cis-$Ru(desazpy)_2Cl_2$	45.08	45.45	16.18	15.34	4.66	5.05

3.2.3.2 Electrospray mass spectrometric data of $Ru(L)_2Cl_2$ complexes

Electrospray mass spectrometry is an important technique to confirm the molecular weight of the complexes. In this work, the data show the different results from ES-MS datas between *trans*- and *cis*-isomers. It is useful for using the results from mass spectra to predict the isomeric compounds that are similar. It will be discussed in details latter.

ES-MS data of the positive ion of a solution of *trans*- and *cis*-$Ru(L)_2Cl_2$ (L =dmsazpy and desazpy) give the fragment ions which are listed in Table 13 for *trans*-$Ru(dmsazpy)_2Cl_2$, Table 14 for *trans*-$Ru(desazpy)_2Cl_2$, Table 15 for *cis*-$Ru(dmsazpy)_2Cl_2$ and Table 16 for *cis*-$Ru(desazpy)_2Cl_2$. The electrospray mass spectra of these complexes are displayed in figure 13-16, respectively.

Table 13 Electrospray mass spectrometric data of *trans*-$Ru(dmsazpy)_2Cl_2$ complex

m/z	Stoichiometry	Equivalent species	Rel. Abun.
624.2	$[Ru(dmsazpy)_2Cl_2+2H-CH_3]^+$	$[M+2H-CH_3]^+$	100
635.2	$[Ru(dmsazpy)_2Cl_2-2H]^+$	$[M-2H]^+$	30
120.9	$[C_6H_4N(CH_3)_2]^+$	$[M-C_6H_4N(CH_3)_2]^+$	77

MW. of the *trans*-$Ru(dmsazpy)_2Cl_2$ complexes = 637.07 = M

The spectrum of *trans*-$Ru(dmsazpy)_2Cl_2$ consists of molecular ion at m/z 624.2 which is two protonation and then lost one methyl group, immediately. This peak is evidence to support the mass of the complex (MW = 637.07). The other fragmentation of m/z 120.9 is attributable to lose one phenyl with substituent $-N(CH_3)_2$.

Table 14 Electrospray mass spectrometric data of *trans*-$Ru(desazpy)_2Cl_2$ complex

m/z	Stoichiometry	Equivalent species	Rel. Abun.
695.1	$[Ru(desazpy)_2Cl_2+2H]^+$	$[M+2H]^+$	60
657.1	$[Ru(desazpy)_2Cl]^+$	$[M-Cl]^+$	30
85.9	$[SNC_3H_3]^+$	$[M-desazpy-N{\equiv}NC_6H_4N(C_2H_5)_2]^+$	100

MW. of the *trans*-$Ru(desazpy)_2Cl_2$ complexes = 693.07 = M

The complex of *trans*-$Ru(desazpy)_2Cl_2$ is not single crystal but the structure can be confirmed to *trans*-configuration based on results of electrospray mass spectrum. The intense peak at m/z 695.1 is assigned to $[Ru(desazpy)_2Cl_2+2H]^+$ ion that is similar to *trans*-$Ru(dmsazpy)_2Cl_2$. This is the main peak that supports the major molecular ion of the complex (MW = 693.07). However, this peak is unstable thus the other fragmentations are obtained. The fragmentation of m/z 657.1 is assigned to the loss chloride and a major stable fragmention at m/z 85.9 which belongs to thiazole ring.

Table 15 Electrospray mass spectrometric data of *cis*-$Ru(dmsazpy)_2Cl_2$ complex

m/z	Stoichiometry	Equivalent species	Rel. Abun.
601.6	$[Ru(dmsazpy)_2Cl]^+$	$[M-Cl]^+$	100
103.4	$[N{\equiv}NC_6H_4]^+$	$[M-NC_2H_2SC-C_6H_4N(CH_3)_2]^+$	63

MW. of the *cis*-$Ru(dmsazpy)_2Cl_2$ complexes = 637.07 = M

The major stable fragment ion at m/z 601.6 which is assigned to the loss chloride atom. The other fragmentation of 103.4 in the positive ion belongs to $[H_4C_6N{\equiv}N]^+$.

Table 16 Electrospray mass spectrometric data of *cis*-$Ru(desazpy)_2Cl_2$ complex

m/z	Stoichiometry	Equivalent species	Rel. Abun.
657.1	$[Ru(desazpy)_2Cl]^+$	$[M\text{-}Cl]^+$	80
695.1	$[Ru(desazpy)_2Cl_2+2H]^+$	$[M+2H]^+$	35
103.8	$[C_6H_5N{\equiv}C]^+$	$[M-ClC_6H_4N(C_2H_5)_2\text{-}\ C_2H_5\text{-}CH_3\text{-}2H]^+$	63

MW. of the *cis*-$Ru(desazpy)_2Cl_2$ complexes = 693.07 = M

Although the single crystals of *cis*-$Ru(desazpy)_2Cl_2$ have not been obtained but the structure of complex can be confirm to be the *cis*-configuration based on results of electrospray mass spectrum. This is due to the pattern of losing chlorine atom to give the major stable fragment ion at m/z 657.1 which is similar to *cis*-$Ru(dmsazpy)_2\ Cl_2$. However, the *cis*-$Ru(desazpy)_2Cl_2$ is unstable at higher ion source energy. It undergoes significant decomposition to give two major species in two pathways. Frist, the molecular ion is two protonated at m/z 695.1. The other species which is the most intense peak at m/z 103.8 is assigned to $[C_6H_5N{\equiv}C]^+$ ion.

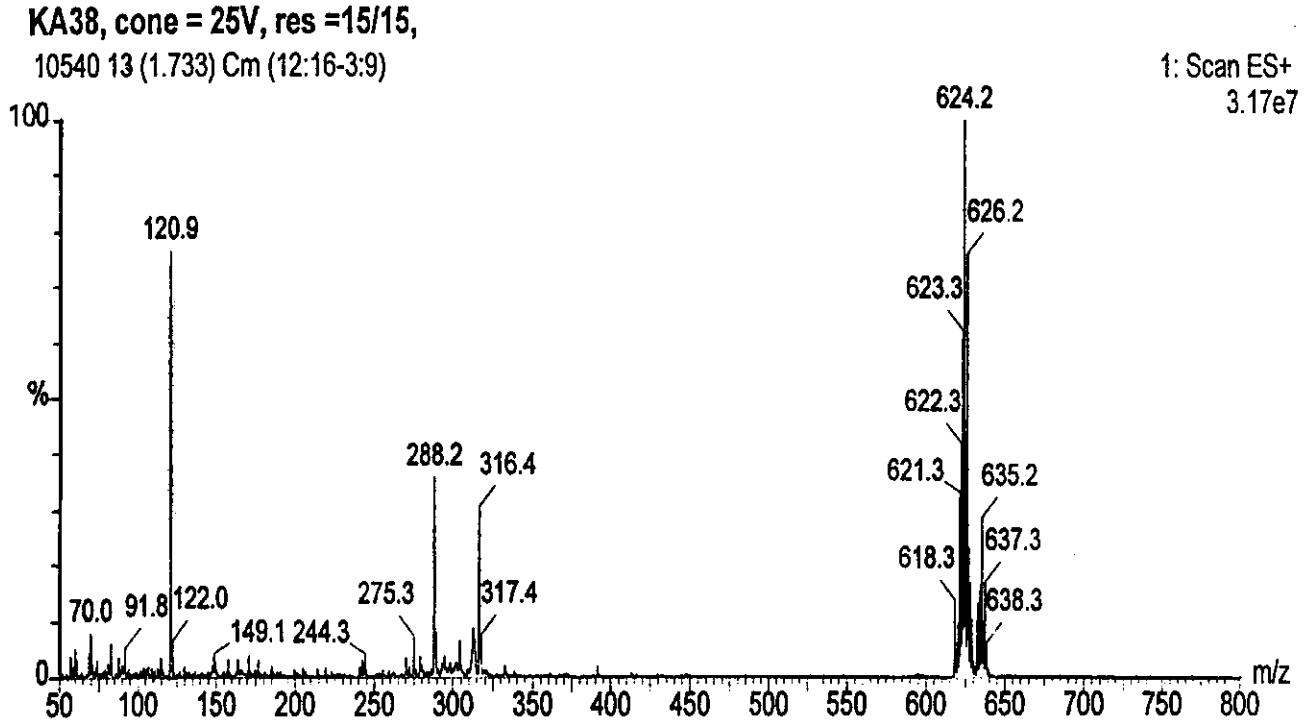

Figure 13 Electrospray mass spectrum of *trans*-Ru(dmsazpy)$_2$Cl$_2$ complex

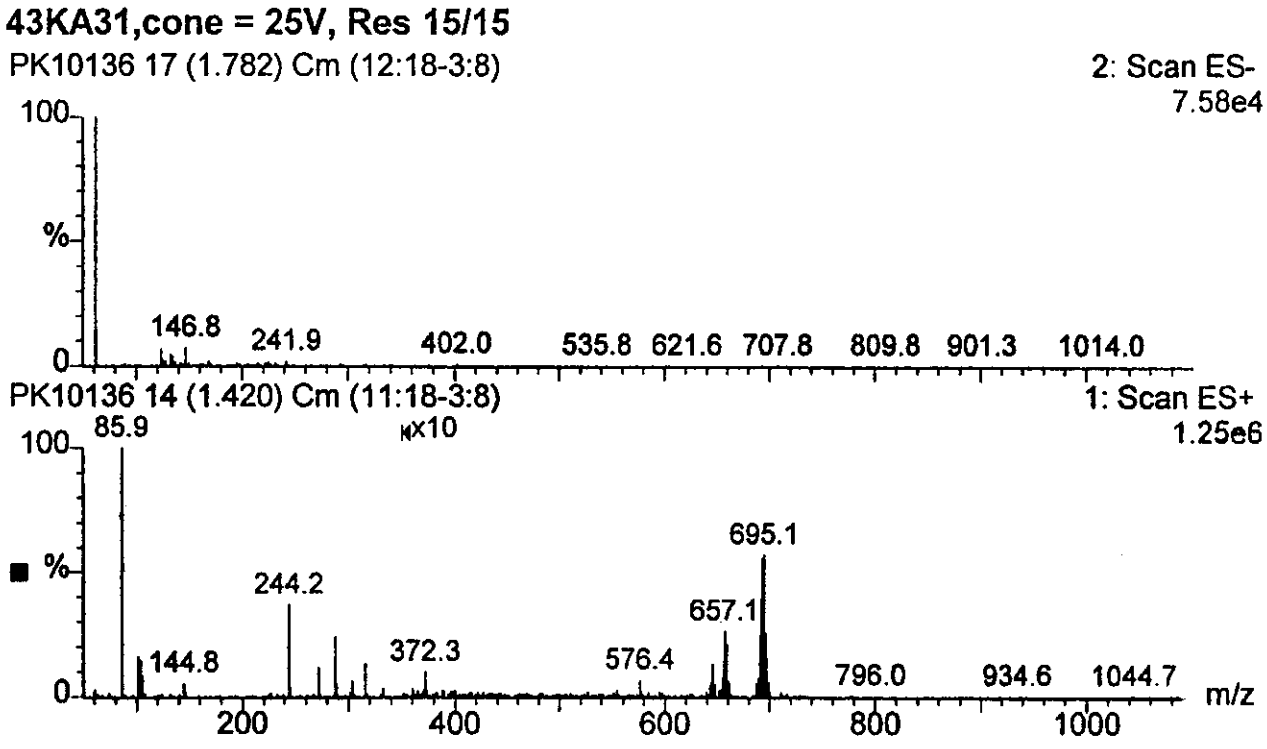

Figure 14 Electrospray mass spectrum of *trans*-Ru(desazpy)$_2$Cl$_2$ complex

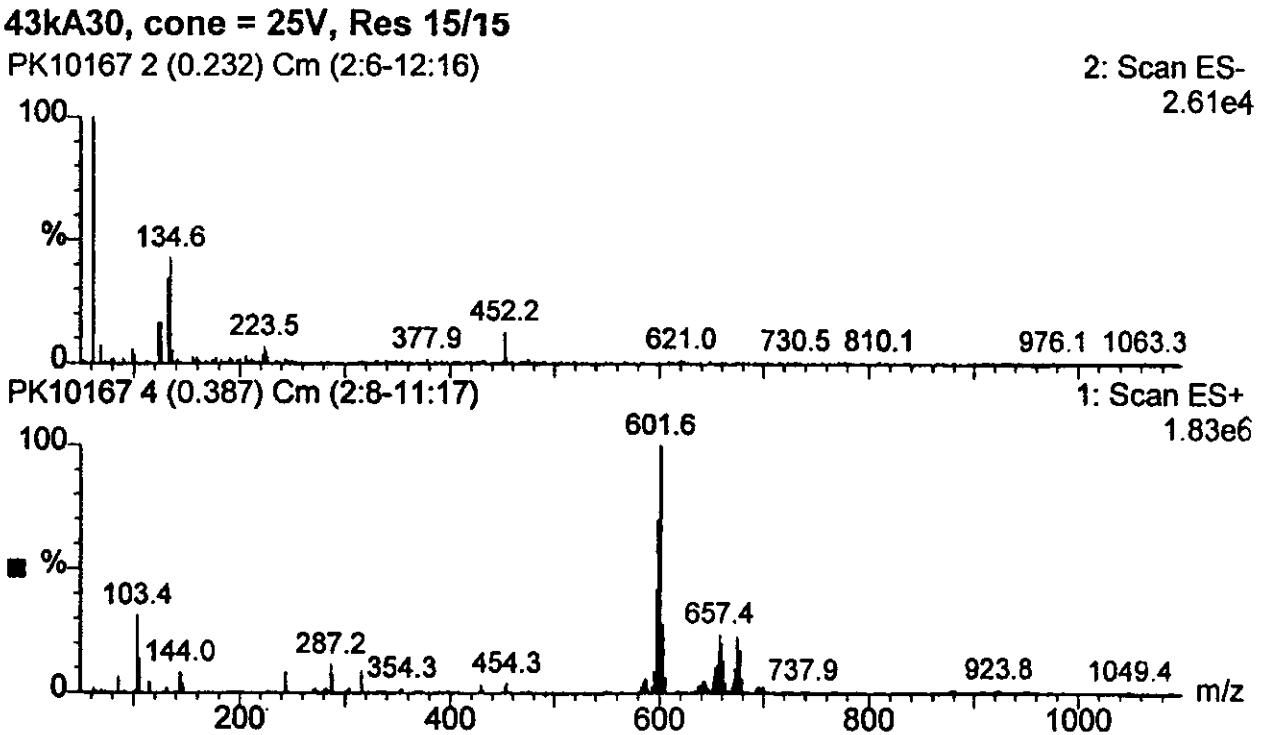

Figure 15 Electrospray mass spectrum of *cis*-Ru(dmsazpy)$_2$Cl$_2$ complex

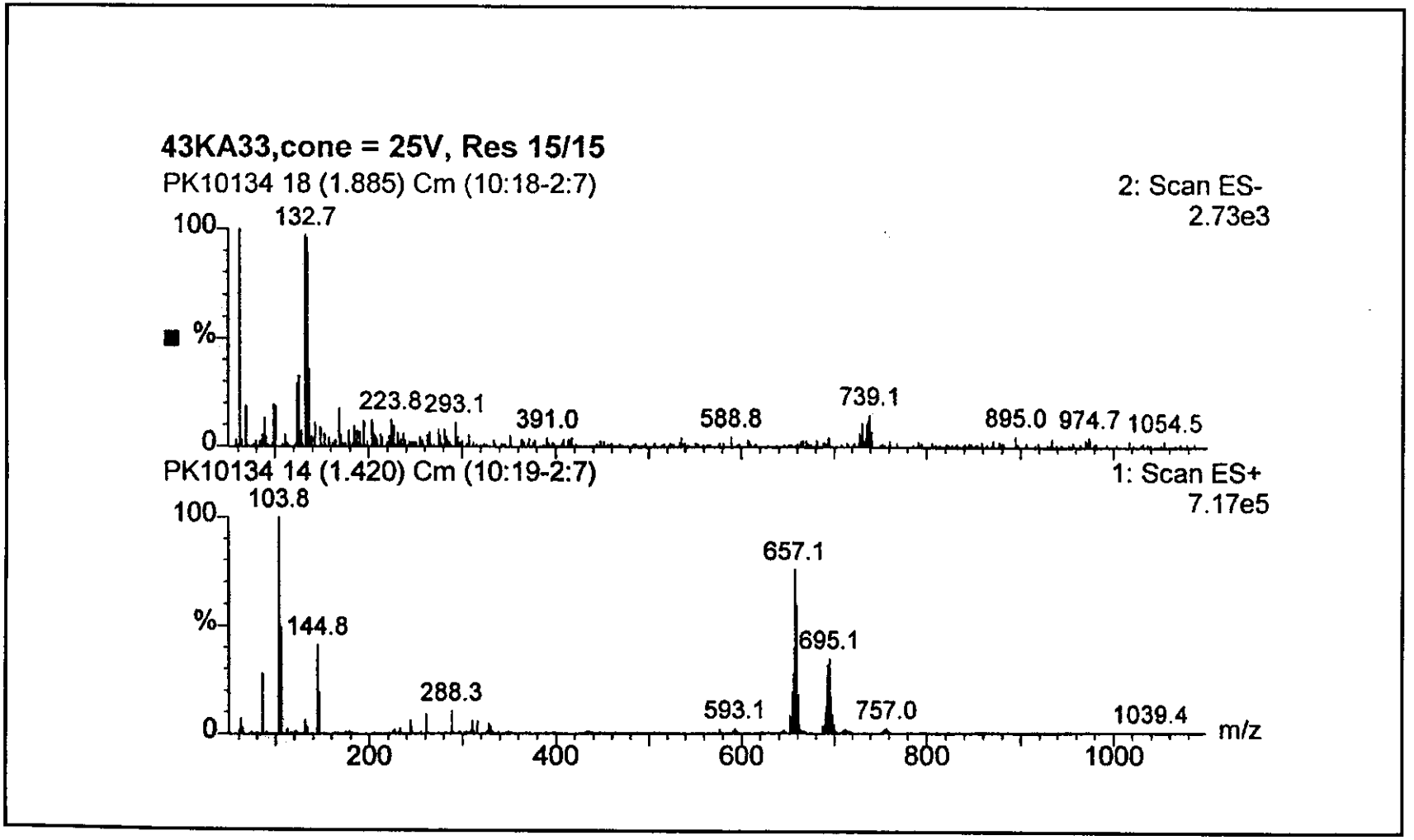

Figure 16 Electrospray mass spectrum of *cis*-Ru(desazpy)$_2$Cl$_2$ complex

3.2.3.3 Infrared spectroscopic data of $Ru(L)_2Cl_2$ (L=dmsazpy and desazpy) complexes

Infrared spectra of $Ru(L)_2Cl_2$ (L=dmsazpy and desazpy) complexes are significant in the range 1600-200 cm^{-1}.Some characteristic frequencies are shown in Table 17 for *trans*-$Ru(dmsazpy)_2Cl_2$, Table 18 for *trans*-$Ru(desazpy)_2Cl_2$, Table 19 for *cis*-$Ru(dmsazpy)_2Cl_2$ and Table 20 for *cis*-$Ru(desazpy)_2Cl_2$. The infrared spectra are shown in figure 17-20, respectively.

Table 17 IR data of *trans*-$Ru(dmsazpy)_2Cl_2$ complex

Compounds	Stretching Modes (cm^{-1})			
	N=N	Ru-N(azo)	Ru-N(th),(py)	Ru-Cl
trans-$Ru(dmsazpy)_2Cl_2$	1244	430	390-410	325
[a]*trans*-$Ru(azpy)_2Cl_2$	1290	368	346	315
dmsazpy	1367	-	-	-
[a]azpy	1424	-	-	-

[a] data from literature review (Krause and Krause, 1980)

Table 18 IR data of *trans*-$Ru(desazpy)_2Cl_2$ complex

Compounds	Stretching Modes (cm^{-1})			
	N=N	Ru-N(azo)	Ru-N(th),(py)	Ru-Cl
trans-$Ru(desazpy)_2Cl_2$	1239	420-430	350-360	320
[a]*trans*-$Ru(azpy)_2Cl_2$	1290	368	346	315
desazpy	1358	-	-	-
[a]azpy	1424	-	-	-

[a] data from literature review (Krause and Krause, 1980)

Table 19 IR data of *cis*-$Ru(dmsazpy)_2Cl_2$ complex

Compounds	Stretching Modes (cm^{-1})			
	N=N	Ru-N(azo)	Ru-N(th),(py)	Ru-Cl
cis-$Ru(dmsazpy)_2Cl_2$	1247	430	390-400	320-340
[a]*cis*-$Ru(azpy)_2Cl_2$	1295	376, 280	358, 268	308, 336
dmsazpy	1367	-	-	-
[a]azpy	1424	-	-	-

[a] data from literature review (Krause and Krause, 1980)

Table 20 IR data of *cis*-$Ru(desazpy)_2Cl_2$ complex

Compounds	Stretching Modes (cm^{-1})			
	N=N	Ru-N(azo)	Ru-N(th),(py)	Ru-Cl
cis-$Ru(desazpy)_2Cl_2$	1249	425	340-350	310-330
[a]*cis*-$Ru(azpy)_2Cl_2$	1295	376, 280	358, 268	308, 336
desazpy	1358	-	-	-
[a]azpy	1424	-	-	-

[a] data from literature review (Krause and Krause, 1980)

In general, characteristic peaks of all isomeric complexes are the sharp single peak of C=N stretching modes which are observed at closed frequencies in the range 1500-1600 cm^{-1}. The N=N stretching frequencies of each isomer of $Ru(L)_2Cl_2$ (L=dmsazpy amd desazpy) complexes are not much different from each other.

The *trans*-$Ru(desazpy)_2Cl_2$ complex shows the N=N mode at lower frequencies than other forms. However, The N=N stretching modes of all complexes

are shifted to lower frequencies from free ligand, indicating the π–acceptor property of the ligands. In comparison with these complexes, the N=N stretching modes of the azpy complexes occurred at higher frequencies than those of the dmsazpy and desazpy complexes. It may be due to the substituents effect in dmsazpy, desazpy ligands which are explained later.

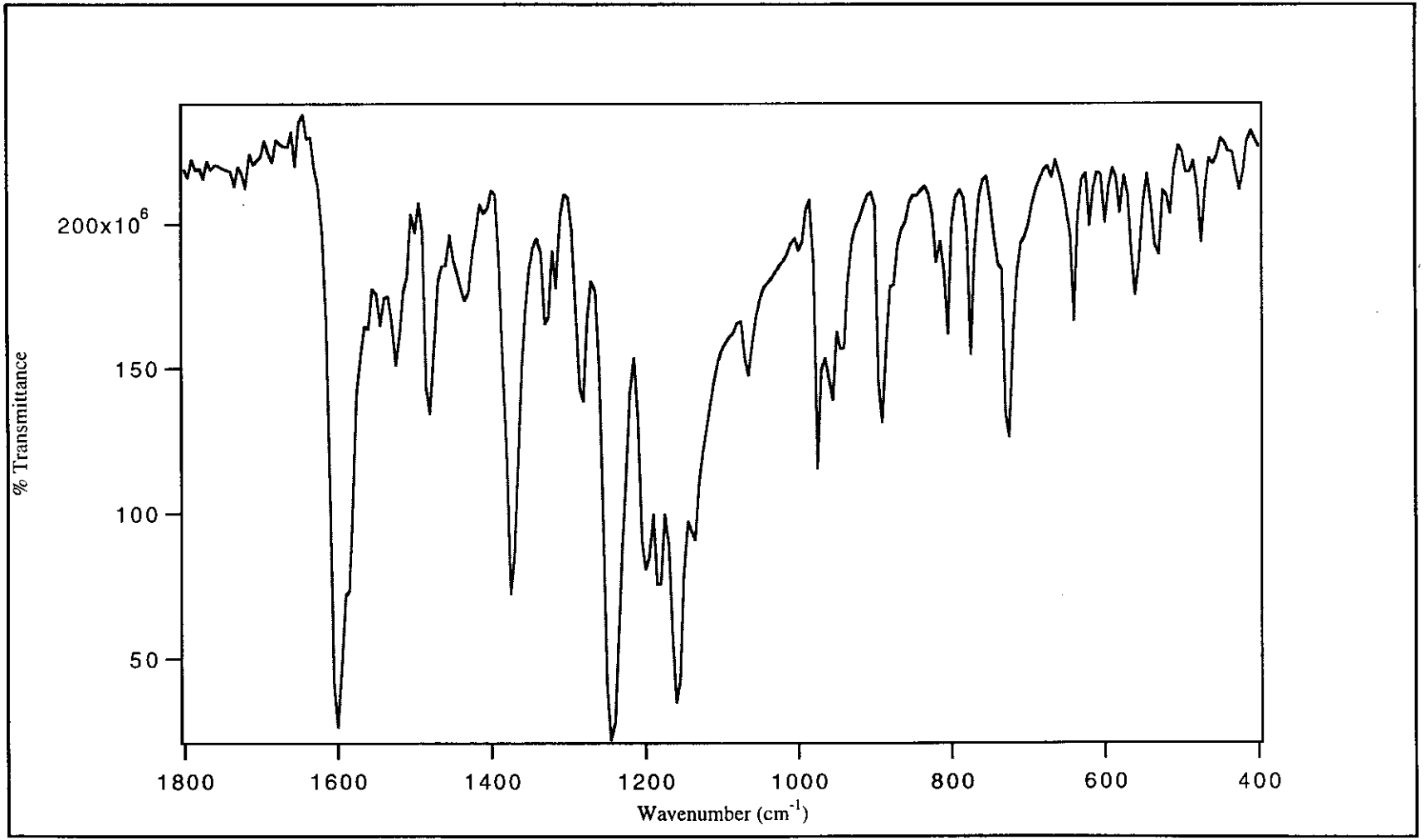

Figure 17 IR spectrum of *trans*-$Ru(dmsazpy)_2Cl_2$ complex

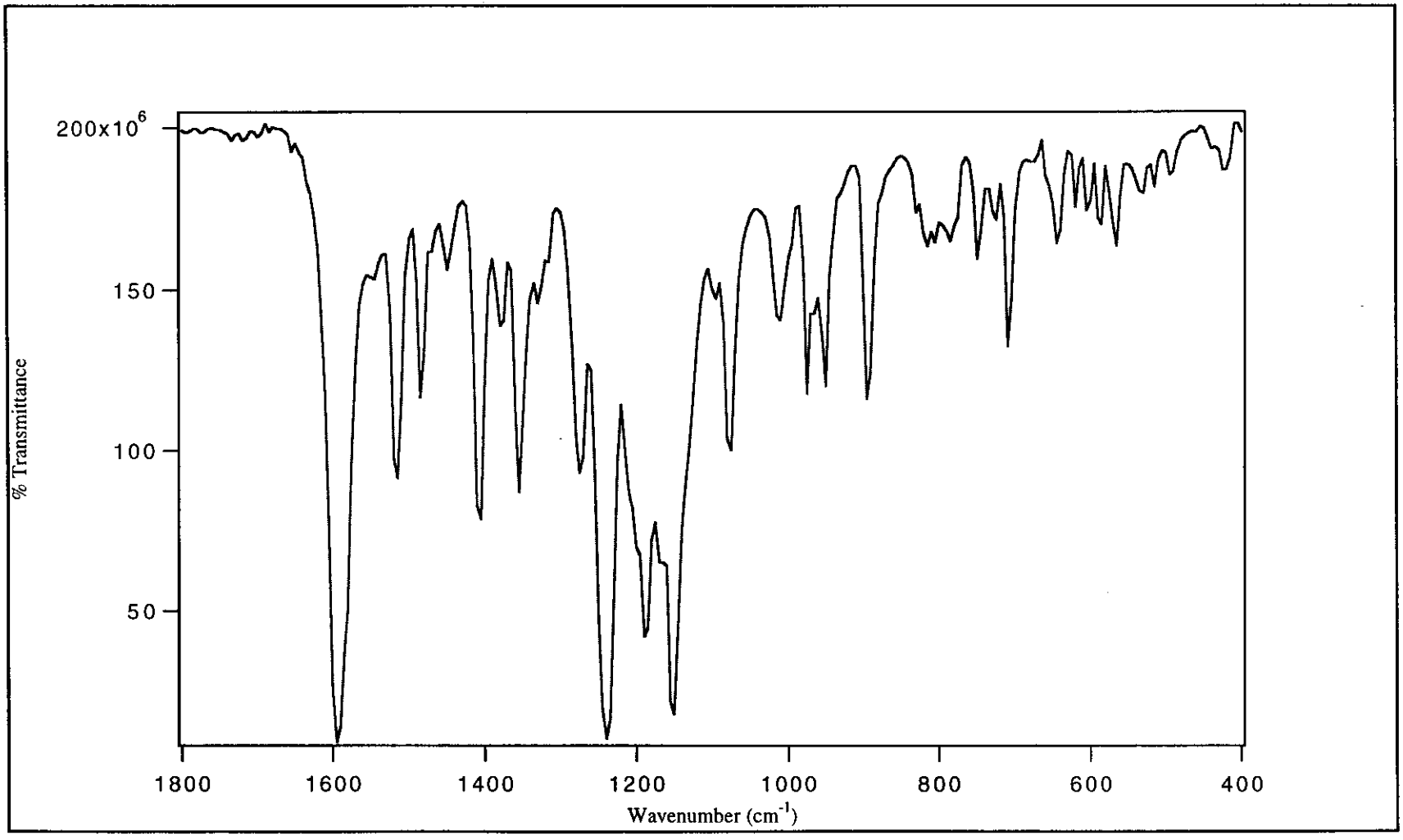

Figure 18 IR spectrum of *trans*-Ru(desazpy)$_2$Cl$_2$ complex

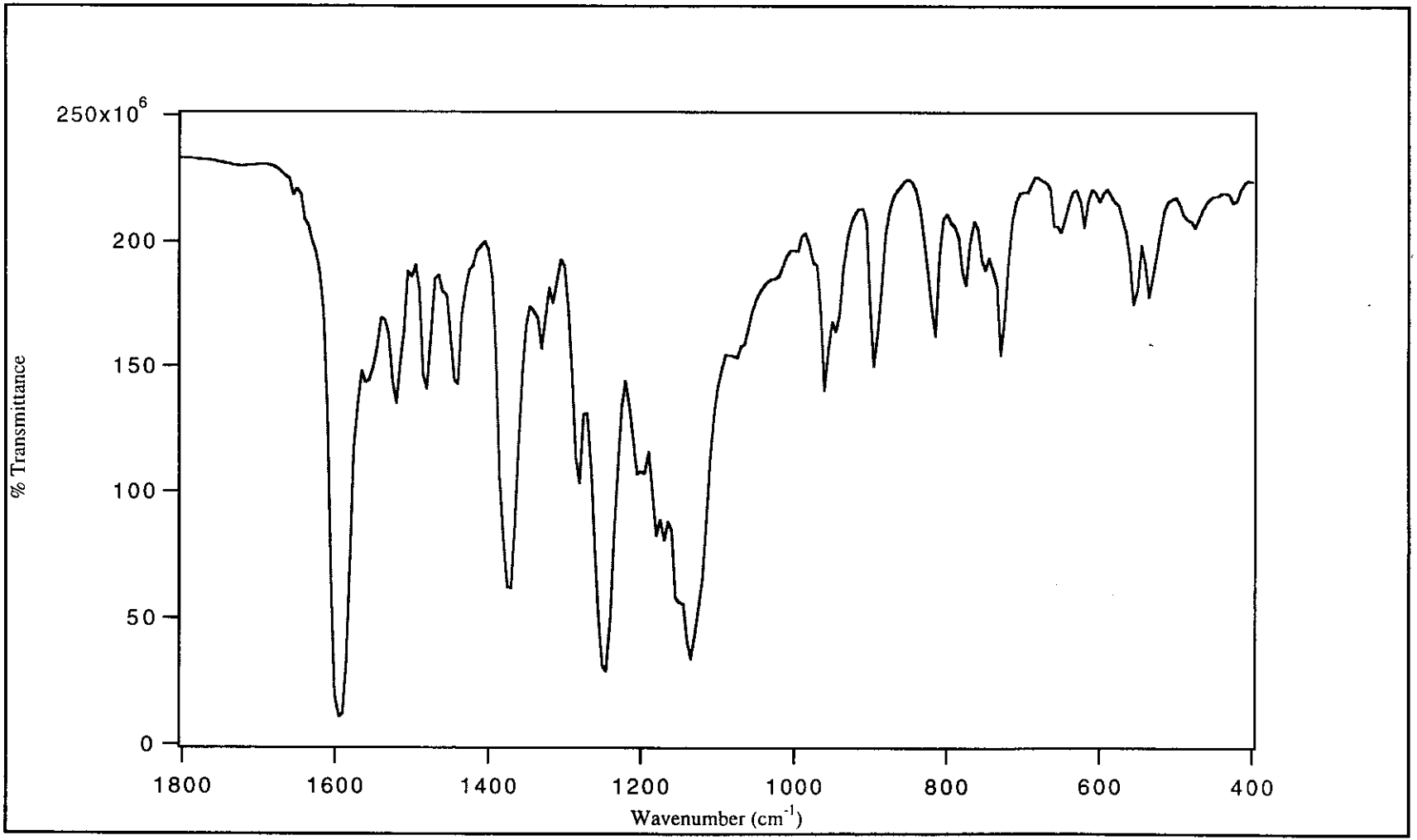

Figure 19 IR spectrum of *cis*-Ru(dmsazpy)$_2$Cl$_2$ complex

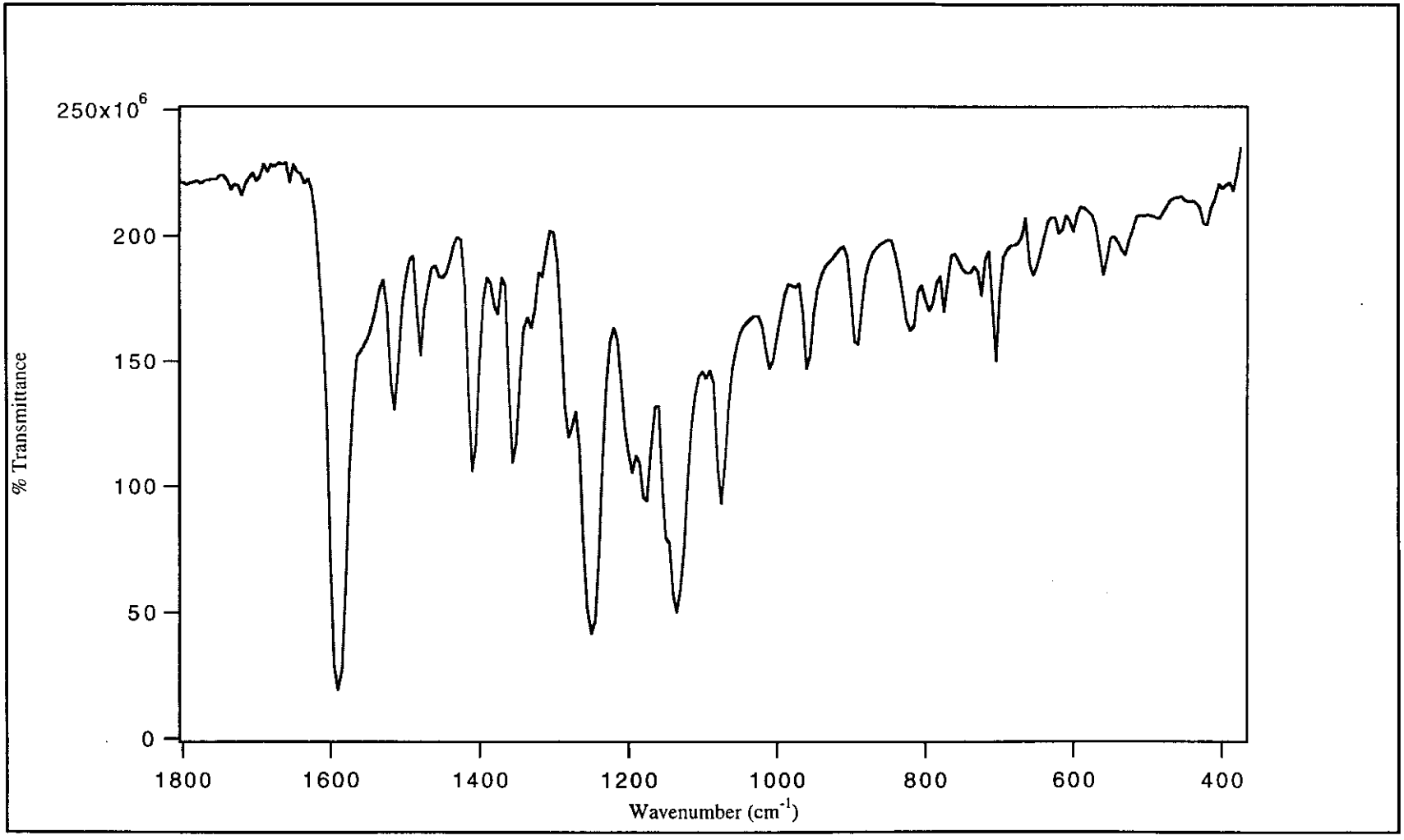

Figure 20 IR spectrum of *cis*-$Ru(desazpy)_2Cl_2$ complex

3.2.3.4 ^{1}H NMR spectrocopic data of $Ru(L)_2Cl_2$ (L= dmsazpy and desazpy) complexes

The ^{1}H NMR spectra are collected in $CDCl_3$ and TMS is used an internal reference. Details of ^{1}H NMR examination of $Ru(L)_2Cl_2$ (L = dmsazpy and desazpy) complexes reveal unusual chemical shifts and simple patterns that prove useful in determining the exact three-dimensional structure and purity of the complexes. The ^{1}H NMR spectra of *trans*- and *cis*-$Ru(L)_2Cl_2$ show only one set of ligand peaks, indicating two equivalent ligands therefore the complexes must be symmetric due to their C_2 axis. The symmetries are C_{2v} for *trans*-$Ru(L)_2Cl_2$ and C_2 for *cis*-$Ru(L)_2L_2$. The proton numbering pattern is shown in Figure 21 for the complex of *trans*-$Ru(L)_2Cl_2$ and in Figure 22 for the complex of *cis*-$Ru(L)_2Cl_2$. The spectral data are given in Table 21 for *trans*-$Ru(dmsazpy)_2Cl_2$, Table 22 for *trans*-$Ru(desazpy)_2Cl_2$, Table 23 for *cis*-$Ru(dmsazpy)_2Cl_2$ and Table 24 for *cis*-$Ru(desazpy)_2Cl_2$. The ^{1}H NMR are displayed in Figure 23-26, respectively.

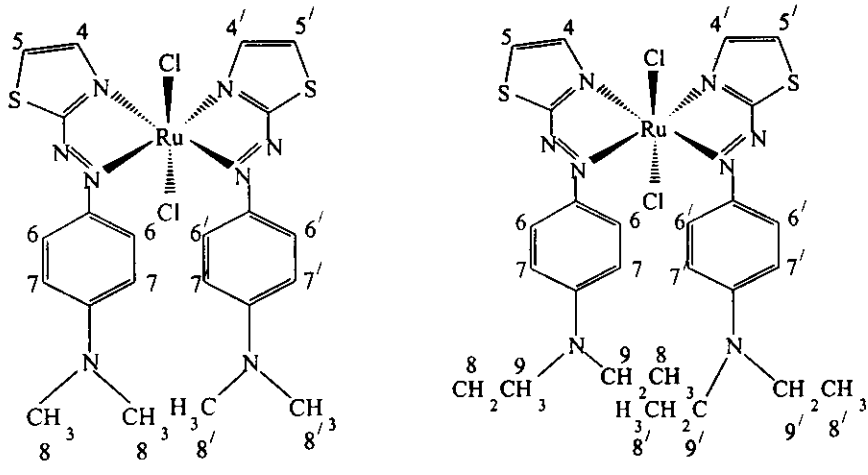

Figure 21 The structures of *trans*-$Ru(dmsazpy)_2Cl_2$ (1) and *trans*-$Ru(desazpy)_2Cl_2$ (2) complexes with proton numbering systems

Table 21 ^{1}H NMR data of *trans*-Ru(dmsazpy)$_2$Cl$_2$ complex

H-position	J-coupling (Hz)	δ (ppm)	Amounts of H	peak
4, 4′	3.5	8.16	2	d
5, 5′	4	7.92	2	d
6, 6′	9	7.53	2	d
7, 7′	9	6.17	2	d
8, 8′	-	3.01	6	s

d = doublet s = singlet

Table 22 ^{1}H NMR data of *trans*-Ru(desazpy)$_2$Cl$_2$ complex

H-position	J-coupling (Hz)	δ (ppm)	Amounts of H	peak
4, 4′	4	8.14	2	d
5, 5′	4	7.86	2	d
6, 6′	9.5	7.68	2	d
7, 7′	9	6.23	2	d
8, 8′	7, 7.5	1.16	6	t
9,9′	7, 7, 7	3.34	4	q

d = doublet s = singlet t = triplet q = quartet

The results from ^{1}H NMR data of the *trans*-Ru(L)$_2$Cl$_2$ reveal that the proton can be divided into five group for *trans*-Ru(dmsazpy)$_2$Cl$_2$ and six group for *trans*-Ru(desazpy)$_2$Cl$_2$. The pattern of ^{1}H NMR signals of *trans*-Ru(L)$_2$Cl$_2$ are different from that of the free ligands. The signal of H-4, 4′ and H-5, 5′ on thiazole ring in complex are shifted to downfield compared to the free ligands. It is due to coordinated

N(th) to ruthenium(II) center and steric effect of structures. In contrast, the H-6, 6′ on phenyl ring are shifted to upfield.

The N-CH_3 signal appears at 3.0-3.3 ppm for those complexes and is downfield shifted compared to free ligands values. The N-CH_2CH_3 groups show a quartet and triplet for -CH_2- and –CH_3 group respectively similar to those of ligand but different chemical shift values.

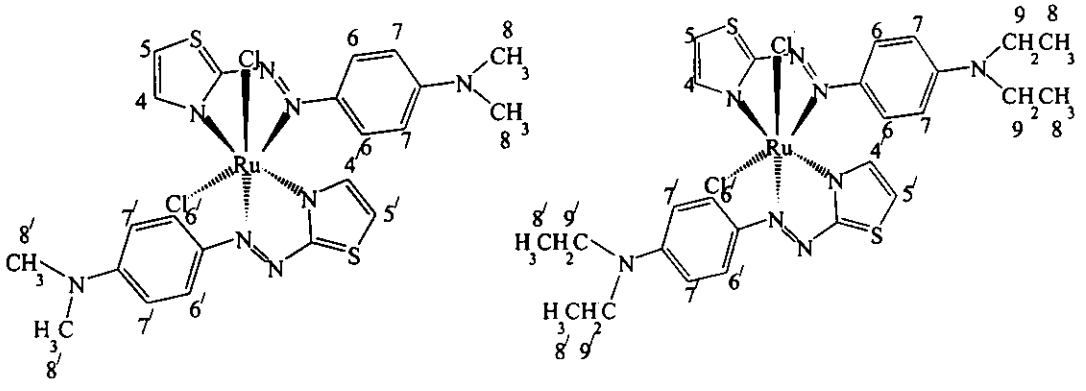

Figure 22 The structures of *cis*-Ru(dmsazpy)$_2$Cl$_2$ (1) and *cis*-Ru(desazpy)$_2$Cl$_2$ (2) complexes with proton numbering systems

Table 23 ^{1}H NMR data of *cis*-Ru(dmsazpy)$_2$Cl$_2$ complex

H-position	J-coupling (Hz)	δ (ppm)	Amounts of H	peak
4, 4′	4	8.53	2	d
5, 5′	4	7.90	2	d
6, 6′	9.5	6.89	2	d
7, 7′	9	6.29	2	d
8, 8′	-	2.99	6	s

d = doublet s = singlet

Table 24 ^{1}H NMR data of *cis*-Ru(desazpy)$_2$Cl$_2$ complex

H-position	J-coupling (Hz)	δ (ppm)	Amounts of H	peak
4, 4′	3.5	8.51	2	d
5, 5′	4	7.86	2	d
6, 6′	9.5	6.88	2	d
7, 7′	9.5	6.26	2	d
8, 8′	3.5, 3.5	1.14	6	t
9, 9′	7, 7.5, 7.5	3.33	4	q

d = doublet s = singlet t = triplet q = quartet

The ^{1}H NMR spectra of *cis*-Ru(dmsazpy)$_2$Cl$_2$ is similar to Ru(desazpy)$_2$Cl$_2$ but differs from *trans*-isomer and the free ligands. The signals of H-4, 4′ on thiazole ring in *cis*-isomer are observed at more 0.37 ppm downfield than that of *trans*-isomer because of the effecting from Cl and nitrogen on thiazole ring in *cis* position. In addition, *cis*-isomer , the H-6, 6′ on phenyl ring is significantly more upfield than that of *trans*-isomer. This is shifted from that of free ligands about 1.04 ppm and from *trans*-Ru(L)$_2$Cl$_2$ about 0.70 ppm that may be due to the effect of different stereochemically.

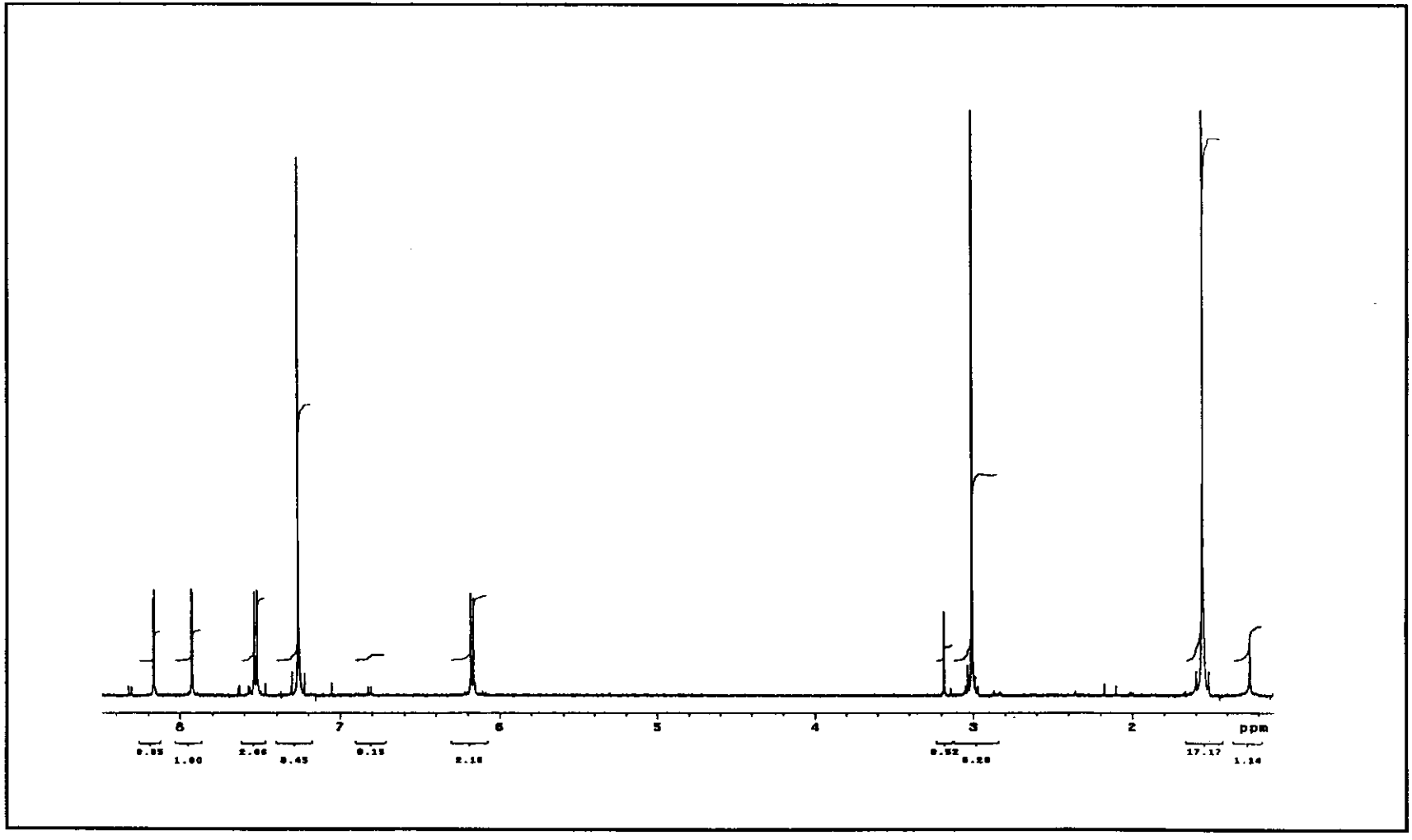

Figure 23 ^{1}H NMR spectrum of *trans*-Ru(dmsazpy)$_2$Cl$_2$ complex

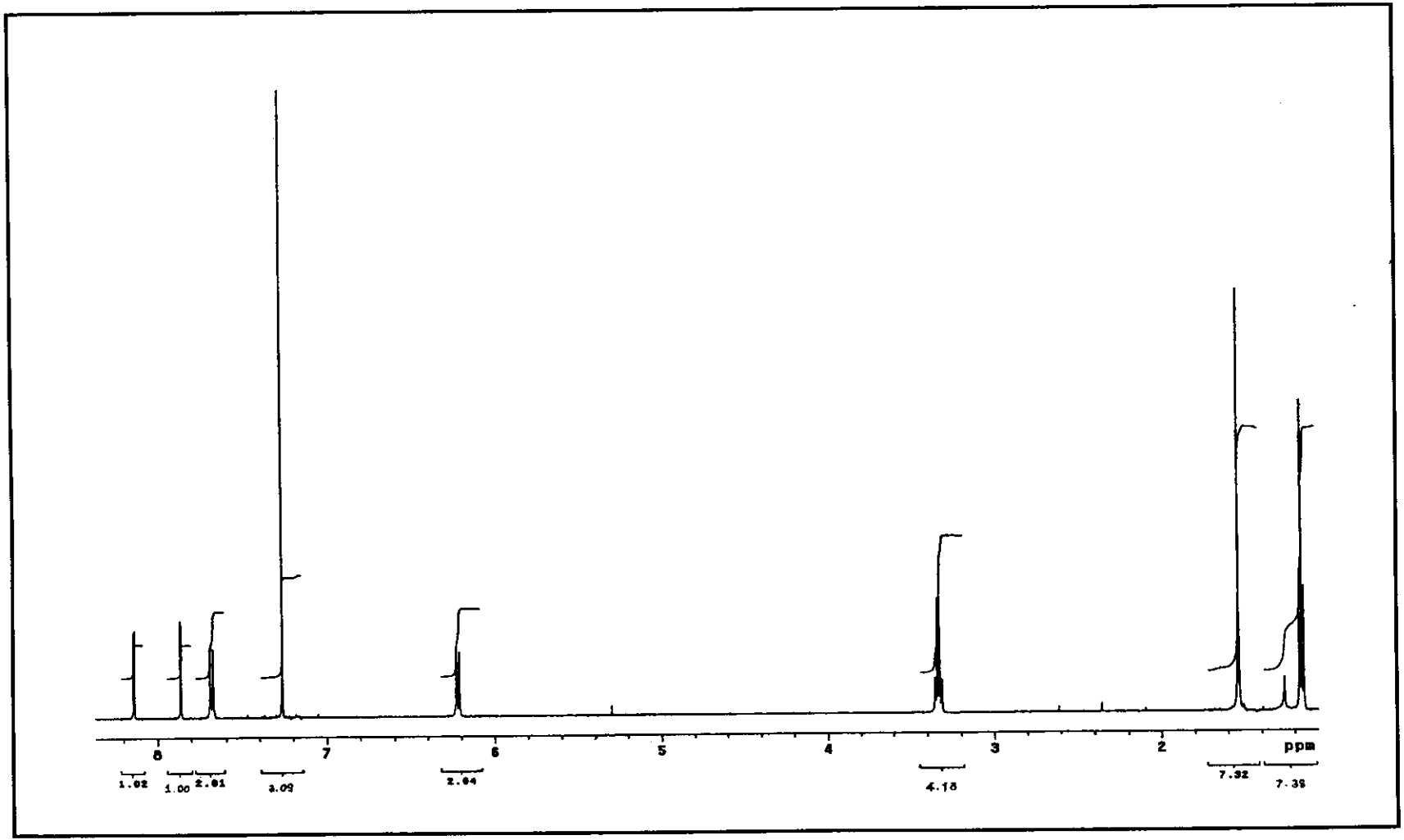

Figure 24 ^{1}H NMR spectrum of *trans*-Ru(desazpy)$_2$Cl$_2$ complex

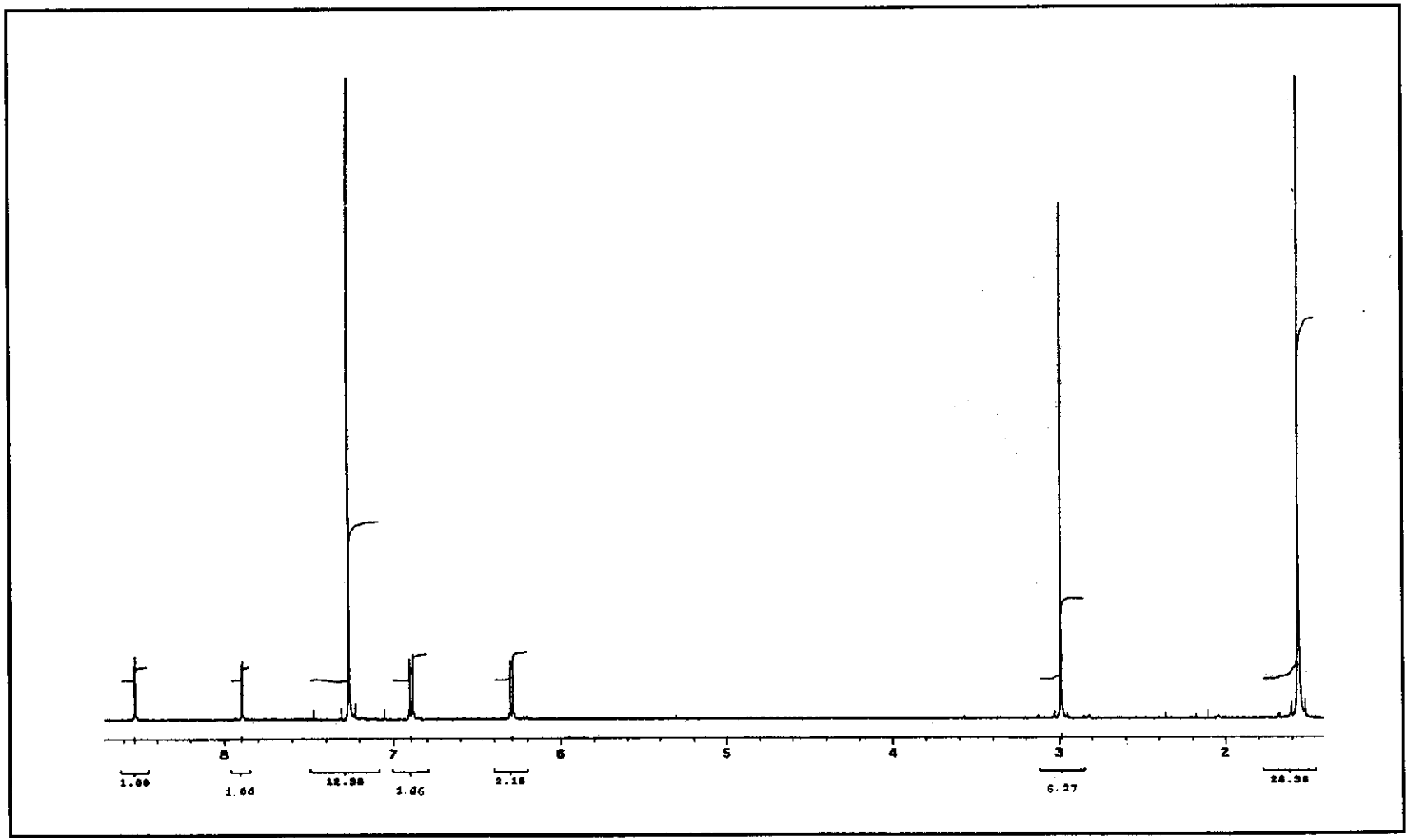

Figure 25 ^{1}H NMR spectrum of *cis*-Ru(dmsazpy)$_2$Cl$_2$ complex

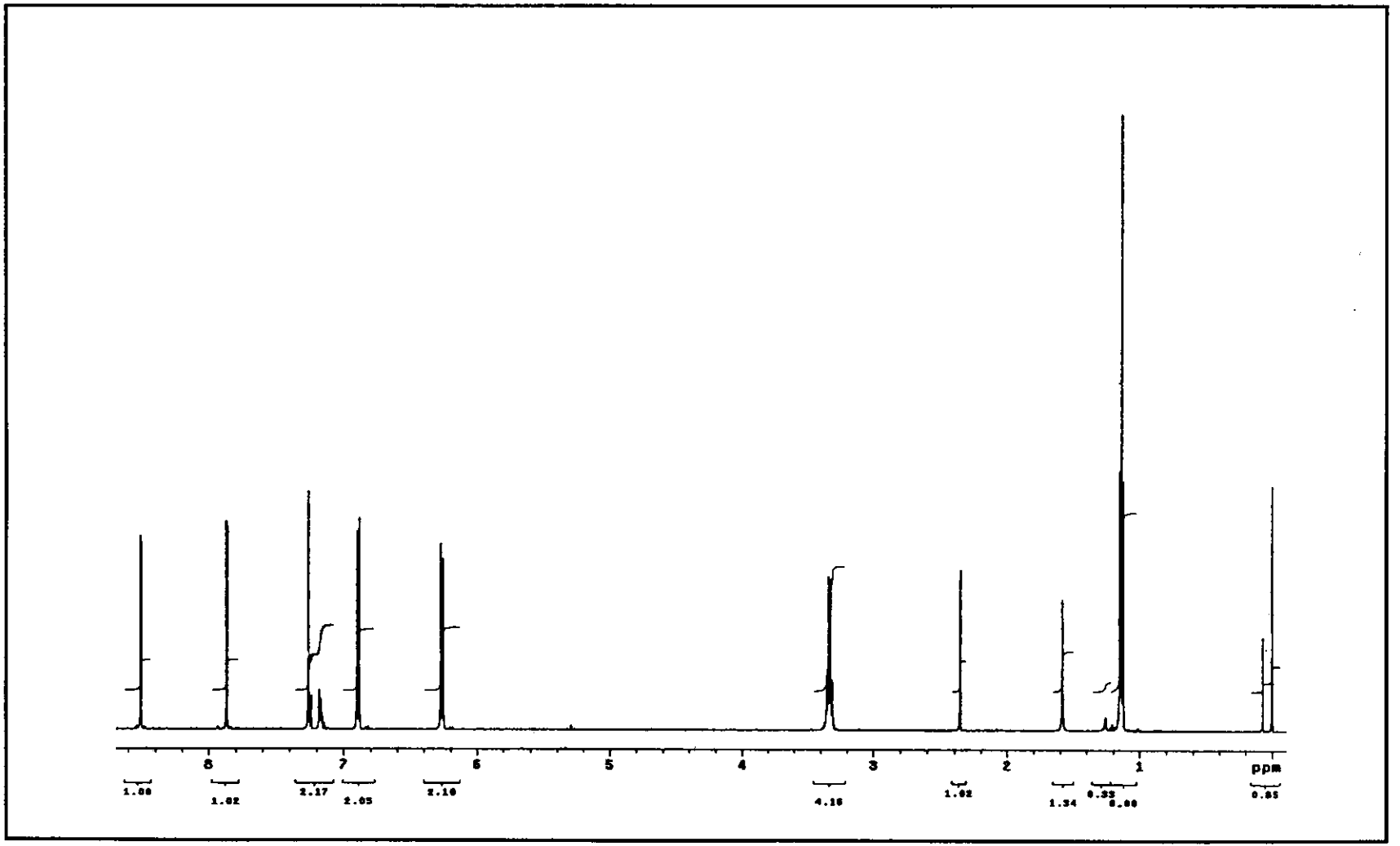

Figure 26 ^{1}H NMR spectrum of *cis*-Ru(desazpy)$_2$Cl$_2$ complex

3.2.3.5 UV-Visible absorption spectroscopic results of $Ru(L_2)Cl_2$ (L=dmsazpy and desazpy)

The absorption spectra of $Ru(L_2)Cl_2$ (L=dmsazpy and desazpy) complexes are studied in the range 200-820 nm of various solvent. The absorption data of all complexes are summarized in Table 25 for *trans*-$Ru(dmsazpy)_2Cl_2$, Table 26 for *trans*-$Ru(desazpy)_2Cl_2$, Table 27 for *cis*-$Ru(dmsazpy)_2Cl_2$ and Table 28 for *cis*-$Ru(desazpy)_2Cl_2$. The spectra of four complexes in visible region are shown in figure 27-30, respectively.

Table 25 UV-Visible spectral data of *trans*-$Ru(dmsazpy)_2Cl_2$ complex

Compounds	Maximum Wavelength, nm (ε^ax 10^{-4}, $M^{-1}cm^{-1}$) in solvents				
	$CHCl_3$	CH_2Cl_2	DMF	DMSO	CH_3CN
trans-$Ru(azpy)_2Cl_2$	410(0.96)	406(1.00)	400(0.91)	404(0.97)	400(0.94)
	632(1.20)	636(1.25)	640(1.13)	644(1.23)	636(1.21)
trans-	490(2.67)	494(2.73)	500(2.89)	502(3.02)	498(2.51)
$Ru(dmsazpy)_2Cl_2$	682(2.87)	692(2.74)	702(2.80)	712(2.90)	698(2.28)

[a]Molar Extinction coefficient

Table 26 UV-Visible spectral data of *trans*-$Ru(desazpy)_2Cl_2$ complex

Compounds	Maximum Wavelength, nm (ε^ax 10^{-4}, $M^{-1}cm^{-1}$) in solvents				
	$CHCl_3$	CH_2Cl_2	DMF	DMSO	CH_3CN
trans-$Ru(azpy)_2Cl_2$	410(0.96)	406(1.00)	400(0.91)	404(0.97)	400(0.94)
	632(1.20)	636(1.25)	640(1.13)	644(1.23)	636(1.21)
trans-	504(3.74)	508(3.65)	512(3.35)	516(4.08)	512(3.48)
$Ru(desazpy)_2Cl_2$	688(3.14)	694(2.86)	698(2.59)	704(3.23)	698(2.48)

[a]Molar Extinction coefficient

Table 27 UV-Visible spectral data of *cis*-$Ru(dmsazpy)_2Cl_2$ complex

Compounds	Maximum Wavelength, nm (ε^a x 10^{-4}, $M^{-1}cm^{-1}$) in solvents				
	$CHCl_3$	CH_2Cl_2	DMF	DMSO	CH_3CN
cis-$Ru(azpy)_2Cl_2$	[b]588(1.14)	-	-	[b]588(1.14)	-
cis-	506(4.98)	510(4.95)	514(5.08)	516(5.22)	508(4.10)
$Ru(dmsazpy)_2Cl_2$	662(2.11)	672(2.01)	680(2.07)	684(2.23)	-

[a]Molar Extinction coefficient. [b]data from literature review (Krause and Krause, 1980)

Table 28 UV-Visible spectral data of *cis*-$Ru(desazpy)_2Cl_2$ complex

Compounds	Maximum Wavelength, nm (ε^a x 10^{-4}, $M^{-1}cm^{-1}$) in solvents				
	$CHCl_3$	CH_2Cl_2	DMF	DMSO	CH_3CN
cis-$Ru(azpy)_2Cl_2$	[b]588(1.14)	-	-	[b]588(1.14)	-
cis-$Ru(desazpy)_2Cl_2$	510(5.42)	512(5.50)	516(4.93)	518(5.39)	512(4.95)
	674(2.50)	680(2.65)	686(2.19)	690(2.77)	684(2.31)

[a]Molar Extinction coefficient

The absorption spectra of those complexes were recorded in both ultraviolet (200-400 nm) and visible regions (400-820 nm). In the UV region, the absorption spectra show very intense bands, which belong to the electronic transitions of the ligands. In the visible region, each complex exhibits intense ($\varepsilon \sim 10^4$ $M^{-1}cm^{-1}$) bands which referred to charge transfer transition.

In this work, the complexes of $Ru(L)_2Cl_2$ (L = dmsazpy and desazpy) display metal-to-ligand charge transfer (MLCT) with two intense bands. Electronic spectra of *trans*-$Ru(dmsazpy)_2Cl_2$ is similar to those of *trans*-$Ru(desazpy)_2Cl_2$ complexes but

different from those of *cis*-isomer. The *trans*-$Ru(L_2)Cl_2$ (L=dmsazpy and desazpy) (greenish-blue complexes) show the most intense (ε ~25,000-40,000) bands in the range 490-516 nm. In contrast to *cis*-$Ru(L)_2Cl_2$ (L = dmsazpy and desazpy) (pink-purple complexes), they show the most intense (ε ~41,000-55,000) bands in the range 506-518 nm and the weak intense (ε ~20,000) bands in the range 662-690 nm in various solvents. In addition, the lowest energy absorption bands of all complexes are shifted when the polarity of solvent is increased, the absorption occurred at lower energy than that of $Ru(azpy)_2Cl_2$ complexes.

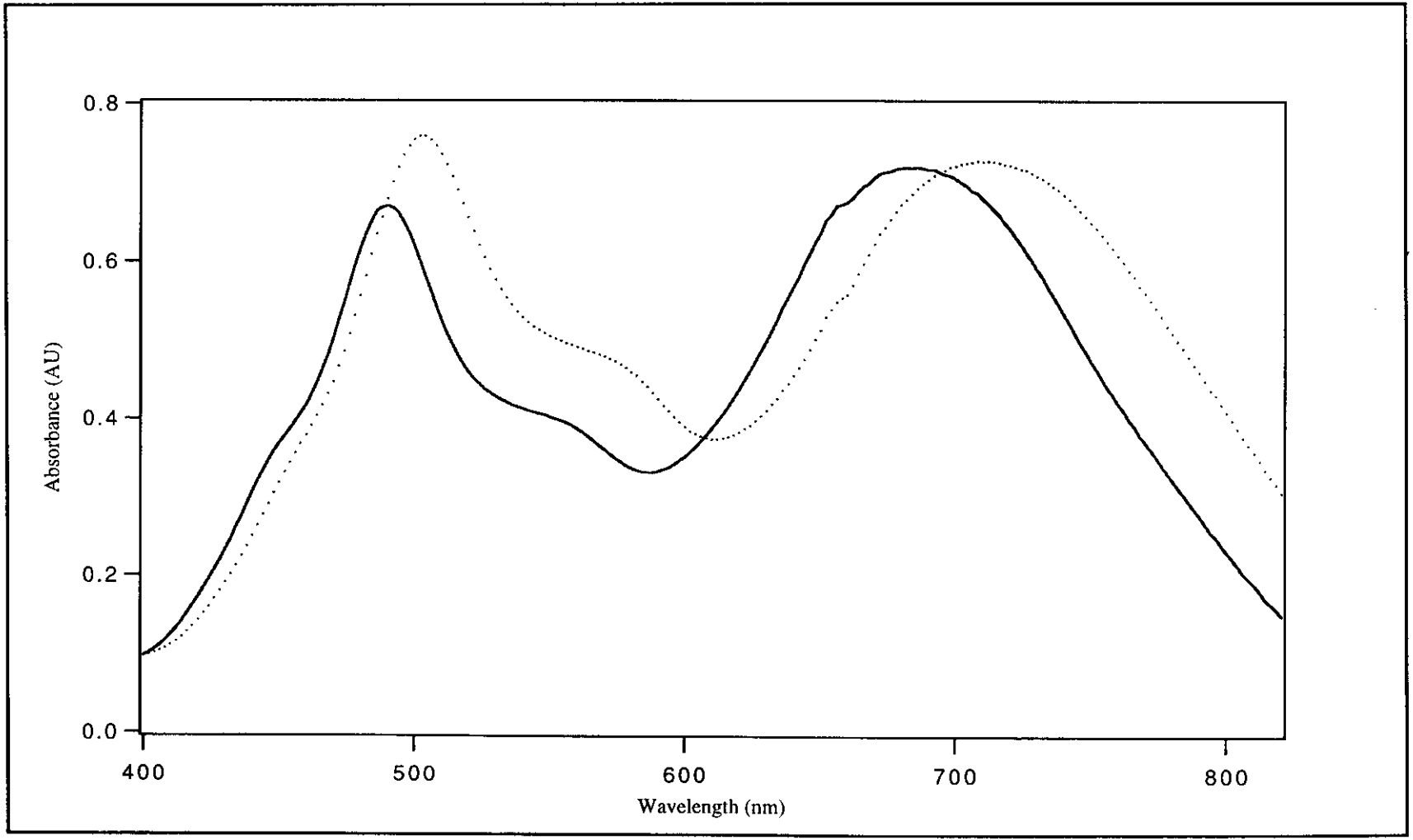

Figure 27 UV-Visible absorption spectra of *trans*-$Ru(dmsazpy)_2Cl_2$ in $CHCl_3$ (__) and dimethyl sulfoxide (....)

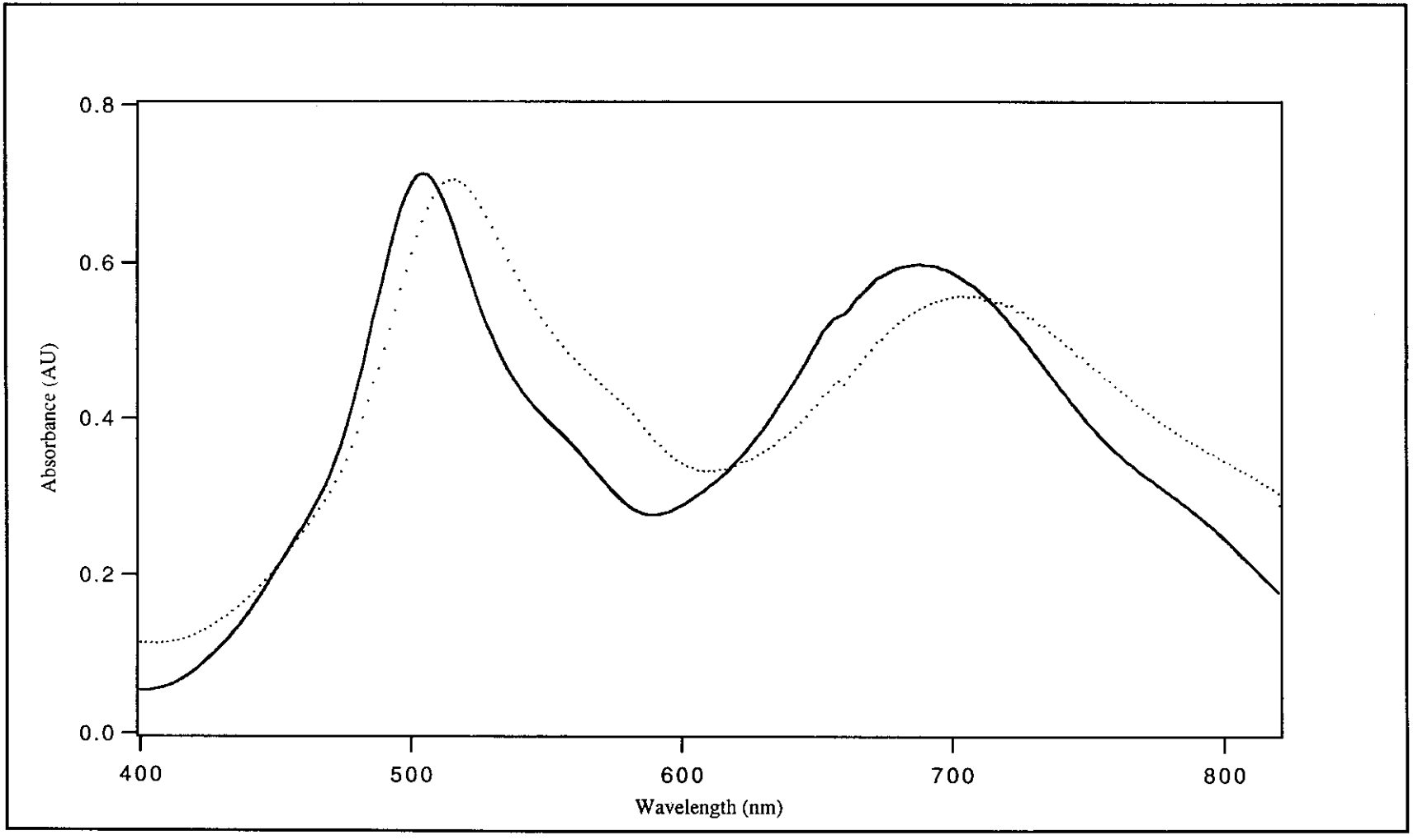

Figure 28 UV-Visible absorption spectra of *trans*-$Ru(desazpy)_2Cl_2$ in $CHCl_3$ (__) and dimethyl sulfoxide (....)

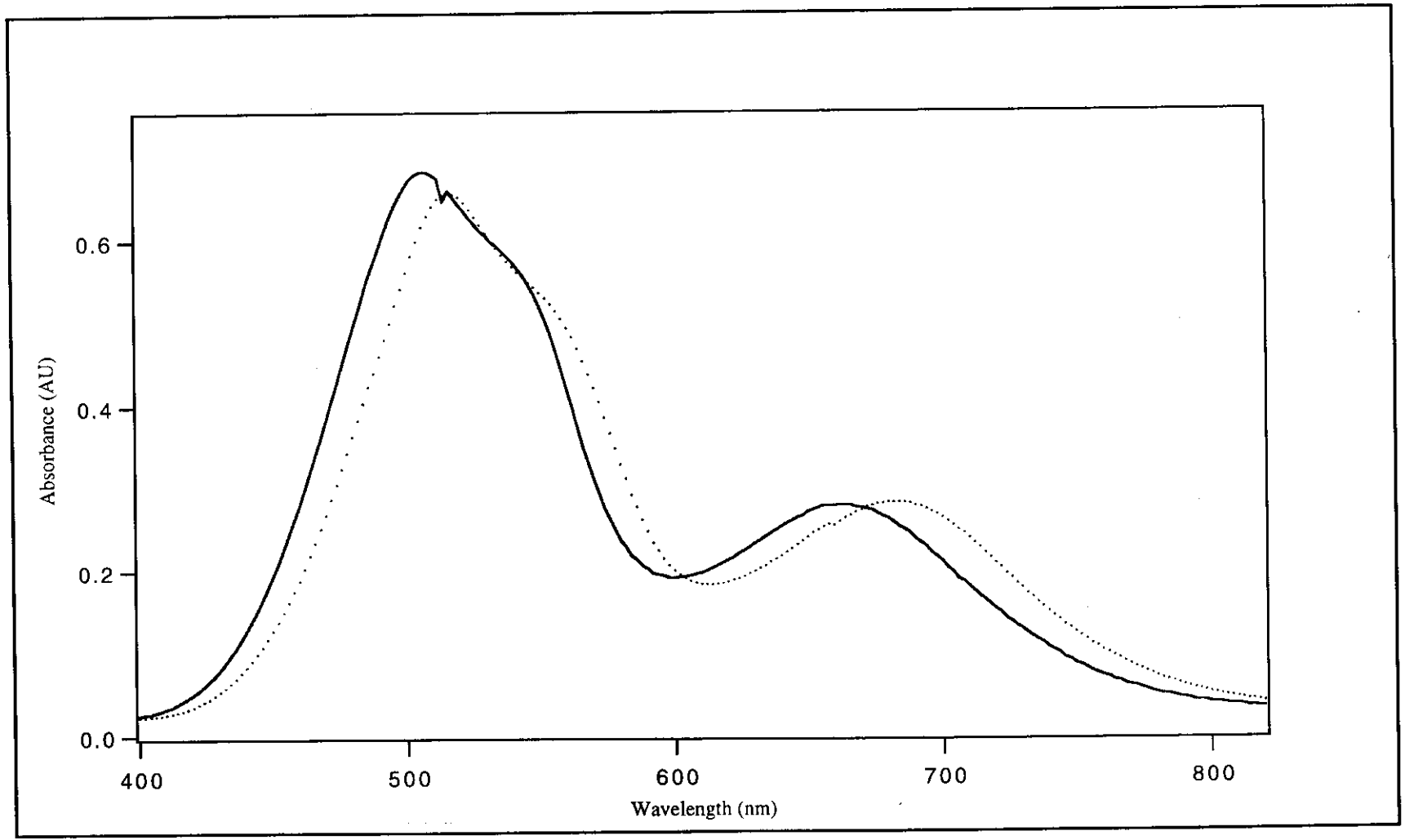

Figure 29 UV-Visible absorption spectra of *cis*-Ru(dmsazpy)$_2$Cl$_2$ in $CHCl_3$ (__) and dimethyl sulfoxide (....)

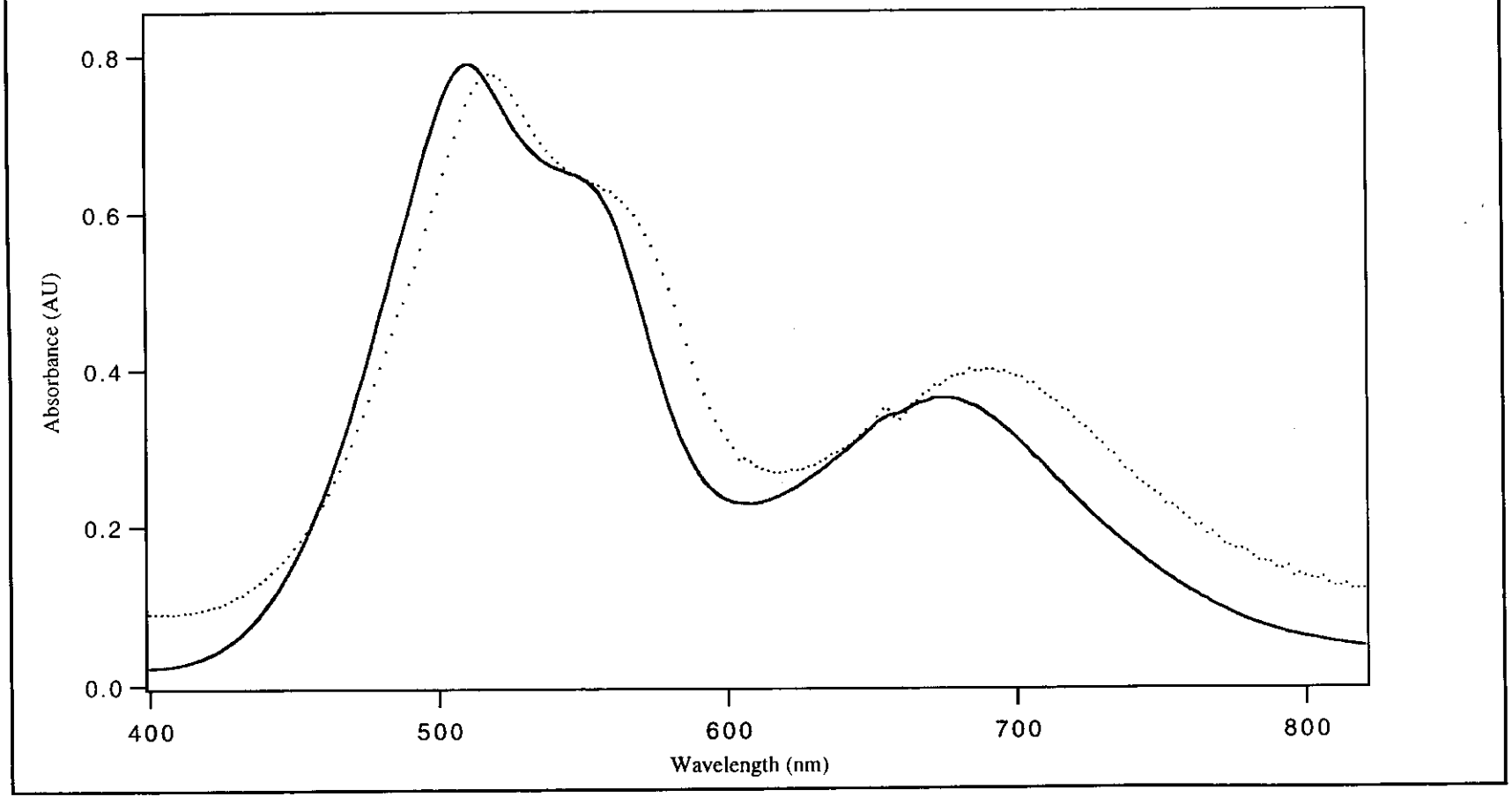

Figure 30 UV-Visible absorption spectra of *cis*-Ru(desazpy)$_2$Cl$_2$ in CHCl$_3$ (__) and dimethyl sulfoxide (....)

3.2.4 X-ray structure of $Ru(dmsazpy)_2Cl_2$ complexes

Recrystallization of the isolated complexes in suitable solvents resulted in good crystal suitable for X-ray diffraction analysis. The structure of those complexes contain a six-coordinated ruthenium atom chelated by two dmsazpy ligands and two chlorides. The atomic arrangement in *trans*-$Ru(dmsazpy)_2Cl_2$ complex involves sequentially two *trans*-chlorides, *cis*-N(th) and *cis*-N(azo) and corresponds to a *trans-cis-cis* configuration. Similarly, the arrangement in *cis*-$Ru(dmsazpy)_2Cl_2$ is *cis-trans-cis*.

3.2.4.1 X-ray structure of *trans*-$Ru(dmsazpy)_2Cl_2$ complex

The single crystals of *trans*-$Ru(dmsazpy)_2Cl_2$ complex are grown in dichloromethane (CH_2Cl_2) solution by slow solvent evaporation at room temperature. The crystal data and collection parameters are listed in Table 29. Selected bond distances and angles are listed in Table 30. View of molecular units of this complex is shown in figure 31.

The coordination sphere around ruthenium is distorted octahedron with varying the angle around ruthenium ion. The average bond angles of atoms in *trans* position of Ru(II) center, Cl(1)-Ru(1)-Cl(2), N(1)-Ru(1)-N(7) and N(5)-Ru(1)-N(3) are in the range 173-177(2)°. This is distorted from linearity by 3-7°, compared with the ideal octahedron (180°). Besides, the orthogonal angles around Ru(II) are in the range 86-94(7)° to 90° in ideal octahedron. This deviation arises from the acute (76.54(9) and 76.44(9)°) chelate bite angles. The phenylazo plane makes an angle 37.1(1) and 36.9(1)° with the chelated azoimine fragment. In addition, two *cis* phenylazo planes are also not parallel, and the dihedral angle is 18.6°.

The average bond distances of Ru-Cl are 2.38(7) Å. The average bond distances of Ru-N(azo), 2.019(2) Å, is shorter than the Ru-N(th) distance, 2.068(2) Å. The N-N bond distance is not available in the dmsazpy ligand . However, the data available in azpy ligand suggest that it is nearly 1.248(3) Å (Panneerselvam *et al.*, 2000). In the complex, the N-N bond distance is 1.323(4) Å. Therefore, the coordination of metal dmsazpy can lead to a decrease in the N-N bond order due to both σ-donor and π-acceptor characters of the ligand. The latter character having more pronounced effect and may be the reason for elongation of N-N bond distance (Misra, *et al.*, 1998).

Furthermore, the complex of *trans*-Ru(dmsazpy)$_2$Cl$_2$ is compared to *trans*-Ru(azpy)$_2$Cl$_2$. Because of the similarity of azoimine groups, it is interesting to study the effect of –N(CH$_3$)$_2$ substituent on complexes and to compare the π–acceptor properties of those ligands. The X-ray result of *trans*-Ru(azpy)$_2$Cl$_2$ is collected in Table 30 and the dihedral angles in different planes of both complexes are given in Table 31.

Table 29 The crystallographic data of *trans*-$Ru(dmsazpy)_2Cl_2$ and *trans*-$Ru(azpy)_2Cl_2$ complexes

Crystal parameters	*trans*-$Ru(dmsazpy)_2Cl_2$	*trans*-$Ru(azpy)_2Cl_2$
Empirical formula	$RuC_{22.50}H_{25}N_8S_2Cl_3$	$RuC_{22}H_{18}N_6Cl_2$
M (g mol^{-1})	679.05	538.39
Crystal color	Dark	Purple
Crystal system	monoclinic	hexagonal
Space group	C2/c	P65
Unit cell dimensions		
a (Å)	30.6120	22.2928(19)
b (Å)	13.1948(1)	22.2928(19)
c (Å)	13.7883	8.5121(10)
α (°)	90	90
β (°)	105.1117(5)	90
γ (°)	90	120
Volume ($Å^3$)	5376.77(3)	3663.5(6)
Z	8	6
Temperature (K)	173(1)	150
Wavelength (Å)	0.71069	0.71073
$Density_{calcd}$ (g cm^{-3})	1.678	1.464
Absorption coefficient (cm^{-1})	10.66	0.9
Param refined	334	281
R %	0.0290	0.0557
R_w %	0.0360	0.1060
Goodness of fit on F^2	1.210	1.190

Table 30 The selected bond distances (Å) and angles (°) and their estimated standard deviations for *trans*-Ru(dmsazpy)$_2$Cl$_2$ and *trans*-Ru(azpy)$_2$Cl$_2$

Distances			
(i) *trans*-Ru(dmsazpy)$_2$Cl$_2$		(ii) *trans*-Ru(azpy)$_2$Cl$_2$	
Ru(1)-Cl(1)	2.380(7)	Ru(1)-Cl(1)	2.377(15)
Ru(1)-Cl(2)	2.379(7)	Ru(1)-Cl(2)	2.368(16)
Ru(1)-N(5)	2.063(2)	Ru(1)-N(1)	2.116(6)
Ru(1)-N(1)	2.073(2)	Ru(1)-N(21)	2.099(5)
Ru(1)-N(7)	2.024(2)	Ru(1)-N(8)	1.986(5)
Ru(1)-N(3)	2.014(2)	Ru(1)-N(28)	1.988(5)
N(5)-C(14)	1.324(3)	N(1)-C(2)	1.356(9)
N(7)-C(15)	1.402(3)	N(8)-C(9)	1.430(9)
N(1)-C(3)	1.326(3)	N(21)-C(22)	1.347(8)
N(3)-C(4)	1.405(3)	N(28)-C(29)	1.450(9)
N(6)-N(7)	1.326(3)	N(7)-N(8)	1.302(8)
N(2)-N(3)	1.321(3)	N(27)-N(28)	1.306(7)
Angles			
Cl(2)-Ru(1)-Cl(1)	173.17(2)	Cl(2)-Ru(1)-Cl(1)	170.50(7)
N(3)-Ru(1)-N(5)	177.72(8)	N(1)-Ru(1)-N(28)	177.52(19)
N(1)-Ru(1)-N(7)	177.88(8)	N(8)-Ru(1)-N(21)	177.40(17)
Cl(1)-Ru(1)-N(5)	91.06(6)	Cl(1)-Ru(1)-N(1)	88.64(14)
Cl(2)-Ru(1)-N(5)	84.37(6)	Cl(2)-Ru(1)-N(1)	85.83(13)
Cl(1)-Ru(1)-N(1)	86.05(6)	Cl(1)-Ru(1)-N(21)	85.71(12)
Cl(2)-Ru(1)-N(1)	89.99(6)	Cl(2)-Ru(1)-N(21)	88.15(12)
Cl(1)-Ru(1)-N(3)	90.96(6)	Cl(1)-Ru(1)-N(28)	88.88(13)

Cl(2)-Ru(1)-N(3)	93.52(6)	Cl(2)-Ru(1)-N(28)	96.63(13)
Cl(1)-Ru(1)-N(7)	92.01(6)	Cl(1)-Ru(1)-N(8)	96.87(13)
Cl(2)-Ru(1)-N(7)	91.86(6)	Cl(2)-Ru(1)-N(8)	89.34(13)
N(5)-Ru(1)-N(7)	76.52(8)	N(1)-Ru(1)-N(8)	76.40(2)
N(3)-Ru(1)-N(1)	76.44(8)	N(28)-Ru(1)-N(21)	75.80(19)
N(3)-Ru(1)-N(7)	104.47(8)	N(28)-Ru(1)-N(8)	103.80(2)
N(5)-Ru(1)-N(1)	102.64(8)	N(1)-Ru(1)-N(21)	104.10(2)

Table 31 The dihedral angles of different planes in *trans*-Ru(dmsazpy)Cl_2 and in *trans*-Ru(azpy)$_2Cl_2$ complex

Planes	*trans*-Ru(dmsazpy)$_2Cl_2$	*trans*-Ru(azpy)$_2Cl_2$
thiazole-azo	12.5(1)	11.0(3)
(pyridine)	8.9(1)	11.5(4)
azo-phenyl	28.0(1)	51.72(3)
	29.6(1)	55.0(5)
thiazole-phenyl	31.3(1)	52.7(3)
(pyridine)	29.4(1)	54.3(3)
chelate rings	3.2(1)	3.6(3)
phenyl rings	18.6(1)	23.7(2)
thiazole-chelate	10.4(1)	9.4(2)
(pyridine)	9.0(1)	10.5(2)
phenyl-chelate	37.1(1)	58.3(2)
	36.9(1)	60.5(2)

* chelate (Ru-N(1)-C(3)-N(2)-N(3)) and (Ru-N(5)-C(14)-N(6)-N(7))

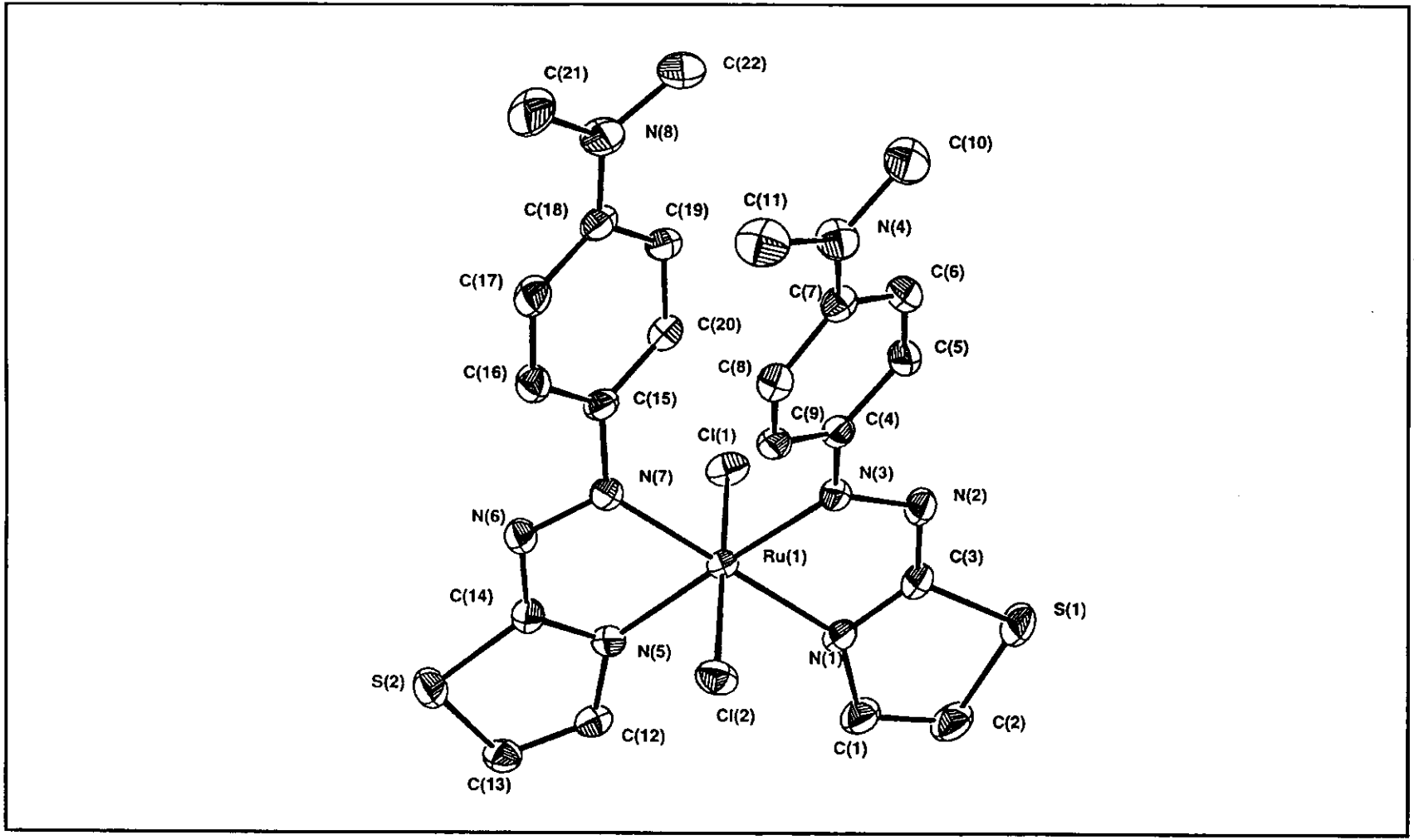

Figure 31 Molecular structure of *trans*-Ru(dmsazpy)$_2$Cl$_2$ complex

3.2.4.2 X-ray structure of *cis*-Ru(dmsazpy)$_2$Cl$_2$ complex

Crystals suitable for X-ray are grown by slow diffusion of toluene into dichloromethane solution of *cis*-Ru(dmsazpy)$_2$Cl$_2$ complex. The crystal data and collection parameters are listed in Table 30. The selected bond distances and angles are summarized in Table 31. View of molecular unit of this complex is shown in figure 32. The molecular structure of *cis*-Ru(dmsazpy)$_2$Cl$_2$ complex is distorted octahedron that one can observed from the *trans* angles around the Ru(II) center, N(5)-Ru(1)-N(1), Cl(1)-Ru(1)-N(7) and Cl(2)-Ru(1)-N(3) are in the range 167-173(7)°. This angles are deviated from *trans* angular value (180°) which arise from the acute chelate bite angles: N(5)-Ru(1)-N(7), 77.41(9)°; N(1)-Ru(1)-N(3), 76.86(9)°. Two chelate planes are deviated from orthogonality (dihedral angle 92.41°) possibly due to steric interaction. Besides, the orthogonal angles around Ru(II) are in the range 85-94(6)°. In addition, the *cis*-chloro angle of 92.71° is close to the ideal octahedral angle of 90° and is comparable to reported values Ru(azpy)$_2$Cl$_2$ complex (89.52°). The dihedral angles of the different planes are shown in Table 32.

The average bond distances of Ru-Cl are 2.409(6) Å. The average bond distances of Ru-N(azo), 2.026 Å, is shorter than the Ru-N(thiazole), 2.035 Å. Furthermore, the N-N bond distance is comparatively shorter than that of *trans*-isomer by 0.005 Å.

Table 32 The crystallographic data of *cis*-Ru(dmsazpy)$_2$Cl$_2$ and *cis*-Ru(azpy)$_2$Cl$_2$ complexes

Crystal parameters	*cis*-Ru(dmsazpy)$_2$Cl$_2$	*cis*-Ru(azpy)$_2$Cl$_2$
Empirical formular	$RuC_{22}H_{24}N_8S_2Cl_2$	$RuC_{22}H_{18}N_6Cl_2$
M (g mol^{-1})	636.58	538.39
Crystal system	triclinic	monoclinic
Space group	$\bar{P}1$	$P2_1/c$
Unit cell dimensions		
a (Å)	9.9921(2)	8.421(8)
b (Å)	10.5018(2)	22.880(2)
c (Å)	13.1927(3)	12.990(2)
α ($^\circ$)	69.431(1)	90
β ($^\circ$)	88.655(1)	116.3(1)
γ ($^\circ$)	79.288(1)	90
V (Å^3)	1272.22(5)	3663.5(6)
Z	2	4
Temperature (K)	173(1)	-
Wavelength (Å)	0.71069	0.71073
Density$_{calcd}$, g cm^{-3}	1.662	1.590
Absorption coefficient (cm^{-1})	10.19	-
Param refined	316	-
R %	0.026	0.051
R_w %	0.036	-
Goodness of fit on F^2	1.08	-

Table 33 The selected bond distances (Å) and angles (°) and their estimated standard deviations for *cis*-Ru(dmsazpy)$_2$Cl$_2$ and *cis*-Ru(azpy)$_2$Cl$_2$

Distances			
(i) *cis*-Ru(dmsazpy)$_2$Cl$_2$		(ii) *cis*-Ru(azpy)$_2$Cl$_2$	
Ru(1)-Cl(1)	2.416(7)	Ru(1)-Cl(1)	2.401(1)
Ru(1)-Cl(2)	2.402(6)	Ru(1)-Cl(2)	2.397(1)
Ru(1)-N(5)	2.040(2)	Ru(1)-N(6)	2.051(4)
Ru(1)-N(1)	2.030(2)	Ru(1)-N(3)	2.045(4)
Ru(1)-N(7)	2.012(2)	Ru(1)-N(4)	1.984(4)
Ru(1)-N(3)	2.041(2)	Ru(1)-N(1)	1.977(4)
N(5)-C(14)	1.328(3)	-	-
N(7)-C(15)	1.400(3)	-	-
N(1)-C(3)	1.323(3)	-	-
N(3)-C(4)	1.409(3)	-	-
N(6)-N(7)	1.324(3)	N(4)-N(5)	1.283(6)
N(2)-N(3)	1.314(3)	N(1)-N(2)	1.279(7)
Angles			
N(5)-Ru(1)-N(1)	173.49(8)	N(3)-Ru(1)-N(6)	-
Cl(1)-Ru(1)-N(7)	168.18(6)	Cl(1)-Ru(1)-N(1)	-
Cl(2)-Ru(1)-N(3)	167.93(6)	Cl(2)-Ru(1)-N(4)	-
Cl(2)-Ru(1)-Cl(1)	92.71(2)	Cl(2)-Ru(1)-Cl(1)	89.52(6)
Cl(1)-Ru(1)-N(1)	85.24(6)	Cl(1)-Ru(1)-N(3)	95.6(1)
Cl(1)-Ru(1)-N(5)	91.03(6)	Cl(1)-Ru(1)-N(6)	89.0(1)
Cl(1)-Ru(1)-N(3)	86.92(6)	Cl(1)-Ru(1)-N(1)	-
Cl(2)-Ru(1)-N(1)	91.08(6)	Cl(2)-Ru(1)-N(3)	86.40(1)

Cl(2)-Ru(1)-N(5)	83.75(6)	Cl(2)-Ru(1)-N(6)	96.30(1)
Cl(2)-Ru(1)-N(7)	88.51(8)	Cl(2)-Ru(1)-N(4)	-
N(5)-Ru(1)-N(3)	108.31(8)	N(6)-Ru(1)-N(1)	99.20(2)
N(5)-Ru(1)-N(7)	77.41(8)	N(6)-Ru(1)-N(4)	76.60(2)
N(7)-Ru(1)-N(1)	106.50(8)	N(4)-Ru(1)-N(1)	100.5(2)
N(3)-Ru(1)-N(7)	94.32(8)	N(4)-Ru(1)-N(1)	93.5(2)
N(1)-Ru(1)-N(3)	76.86(8)	N(3)-Ru(1)-N(1)	76.1(2)

Table 34 The dihedral angles of different planes in *cis*-Ru(dmsazpy)$_2$Cl$_2$ and in *cis*-Ru(azpy)$_2$Cl$_2$ complexes

Planes	*cis*-Ru(dmsazpy)$_2$Cl$_2$	*cis*-Ru(azpy)$_2$Cl$_2$
thiazole-azo	6.7(1)	6.4(3)
(pyridine)	31.7(1)	6.9(2)
azo-phenyl	4.9(1)	39.2(3)
	23.7(1)	36.5(3)
thiazole-phenyl	8.9(1)	42.9(1)
(pyridine)	31.7(1)	45.9(1)
chelate rings	92.4(1)	78.8(1)
phenyl rings	78.0(1)	5.8(1)
thiazole-chelate	8.3(1)	3.8(1)
(pyridine)	11.3(1)	7.9(1)
phenyl-chelate	11.4(1)	47.8(2)
	21.8(1)	44.8(1)

*chelate (Ru-N(5)-C(14)-N(6)-N(7)) and (Ru-N(1)-C(3)-N(2)-N(3))

The average N-N bond distances from X-ray data of both complexes are 1.323(2) Å for *trans*-Ru(dmsazpy)$_2$Cl$_2$ complex and 1.319(2) Å for *cis*-Ru(dmsazpy)$_2$ Cl$_2$ complex.

In case of the Ru(azpy)$_2$Cl$_2$ complexes, the average N-N distances are observed at 1.308(8) Å for *trans*-Ru(azpy)$_2$Cl$_2$ complex and 1.281(6) Å for *cis*-Ru(azpy)$_2$Cl$_2$ complex whereas 1.248(2) Å are found in free azpy ligand.

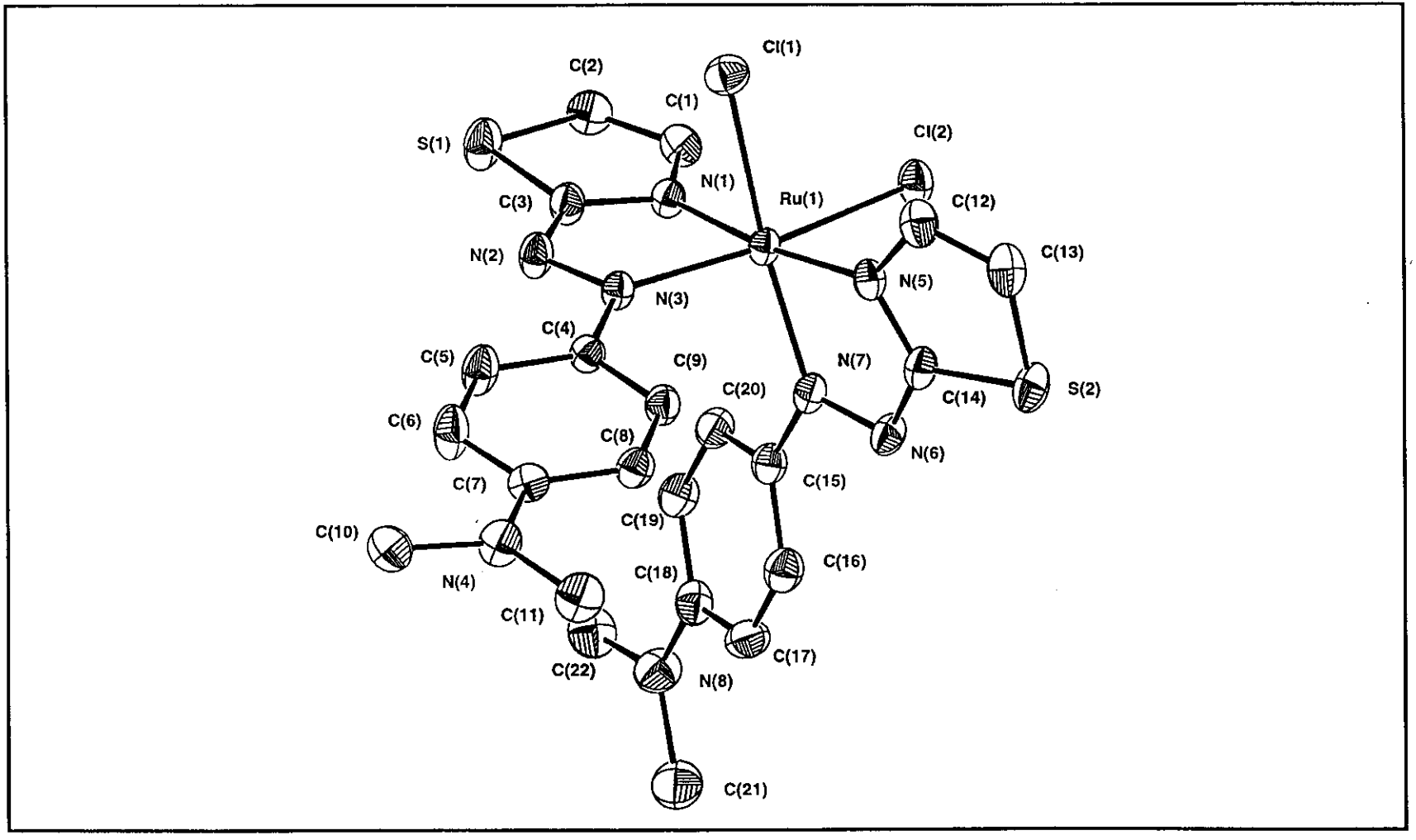

Figure 32 Molecular structure of *cis*-Ru(dmsazpy)$_2$Cl$_2$ complex

3.3 Electrochemistry of complexes

3.3.1 Electrochemistry of dmsazpy and desazpy ligands

The redox behavior of those compounds in acetonitrile solution are examined nusing cyclic voltametry technique with a platinum disk as a working electrode. The potentials are reported with reference to the ferrocene couple ($E_{1/2}$ = 0.0 V, ΔE= 52 mV.) $E_{1/2}$ value are calculated from the average of the anodic and cathodic peak potentials ($E_{1/2} = (E_{pa} + E_{pc})/2$) at scan rate of 50 mV s^{-1} and ΔE value is calculated from the difference of the both of peaks. The voltammograms display metal oxidation at positive side and the ligand reduction at the negative side to the ferrocene. However, the positive potential side is propably the couple of free ligand which may be the substituent effect. The structures of dmsazpy and desazpy were similar to azpy but azpy has no substituent. Therefore, it is interesting for considering the cyclic voltametric data of free ligands frist. The cyclic voltammogram of dmsazpy is similar to desazpy. The three couples of these ligands are observed, one of those is in reduction potential range (negative potential) and the other two are in oxidation potential range (positive potential). Whereas, the azpy ligand has no peaks in positive potential. The result of data from CV was displayed in Table 35, and a representative cyclic voltammogram are shown in Figure 33.

In this work, the difference scan rates are applied to the electrochemical cell for examining redox behavior of those compounds, which give a reversible or irreversible couple. The couple, which give anodic currents equal to cathodic currents, was referred to reversible couple. In contrast, the unequal currents are referred to the transfer of the electron in reduction and oxidation are not equal. This could lead to irreversible reaction.

Table 35 The cyclic voltammetric data of dmsazpy and desazpy ligands in 0.1 M TBAH CH_3CN at scan rate 50 mV/s. (ferrocene used as an internal standard, $\Delta Ep = 54$ mV)

Compound	$E_{1/2}$, V (ΔEp, mV)	
	Oxidation	Reduction
dmsazpy	+0.51[a] +0.82 (40)	-1.54 (58)
desazpy	+0.53[a] +0.83 (48)	-1.56 (78)
azpy	-	-1.58 (171)

a = irreversible anodic peak

Reduction potential

The reduction potential of dmsazpy and desazpy ligangs display reversible couple at $E_{1/2}$ = -1.54 V and -1.56 V at scan rate 50 mV/s. Those ligands are one electron transfer process related to the ΔEp of ferrocene. Comparison with azpy ligand, the reduction potential displays a reversible couple at $E_{1/2}$ = -1.58 V which are two electron transfer process related to the ΔEp of ferrocene.

Oxidation potential

In the potential 0 to +1.30 V, the cyclic voltammograms of dmsazpy and desazpy ligands show the irreversible anodic peak at +0.51 V and +0.54 V, respectively eventhough high scan rates (100, 200, 500,1000 mV/s) were applied. Another one couple in this range is occurred at +0.82 V (40) for dmsazpy and

+0.83 (48) for desazpy. This couple could not individually arise at low scan rates but this couple could arise at higher scan rates (200, 500 and 1000 mV). These characteristics of two couples of both ligands are described as below.

The couple I is only anodic peak studied in the range 0.30-0.90 V. The cyclic voltammogram show the irreversible couple eventhough the various scan rate are applied (100, 200, 500, 1000 mV/s). This peak could occur spontaneously. (Figure 37 Appendix C).

The couple II was studied in the range 0.78-1.10 V. The cyclic voltammogram showed that this couple could not individually arise at low scan rate but at higher scan rates, this couple could arise (Figure 38 Appendix C).

The results of those ligands are different from that of azpy ligand. There is no peaks in oxidation potential but only one couple in reduction potential. Thus, it can easily determine the Ru(II/III) couple in the $Ru(azpy)_2Cl_2$ complexes.

The different couples in oxidation potential of dmsazpy and desazpy may be due to substituent effects. For clearly that of these results, we study the substituent effect on those ligand structure from starting material (*N,N*-dimethylaniline and *N,N*-diethylaniline) which are used to synthesize those ligands. The results show clearly that it has one irreversible couple in the oxidation potential which was nearly the position of couple I in ligands (figure 39 Appendix C). Thus, it can confirm that oxidative couples arise from the substituent groups. In addition, couple II of these ligands may be due to the characteristic of azo function group, not from starting material because it can occur from the only couple I species.

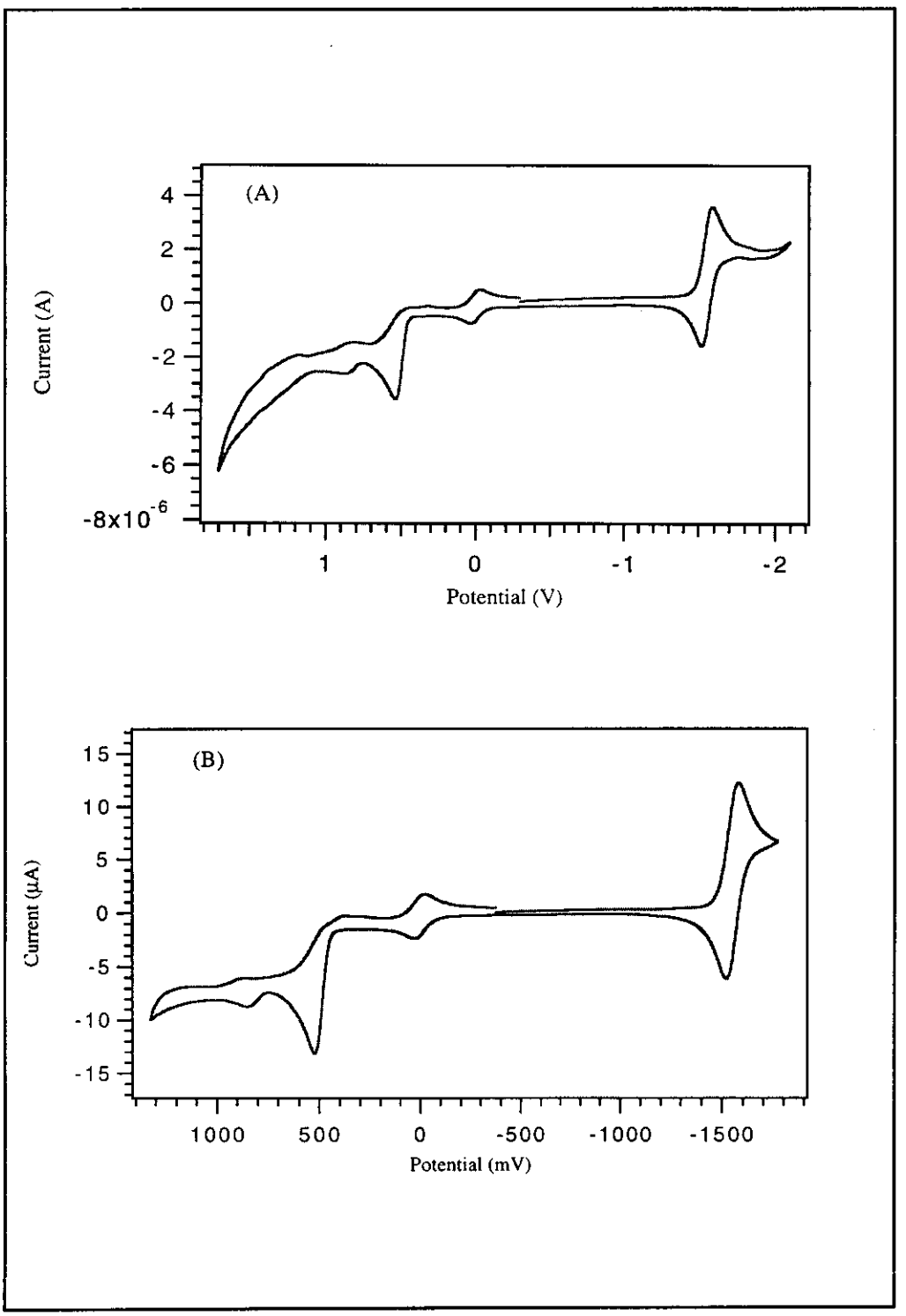

Figure 33 Cyclic voltammograms of (A) dmsazpy and (B) desazpy in 0.1 M TBAH CH_3CN at scan rate 50 mV/s

3.3.2 The $Ru(L)_2Cl_2$ (L=dmsazpy and desazpy) complexes.

The cyclic voltammetric data of all complexes are shown in Table 36. The complexes of $Ru(L)_2Cl_2$ are electroactive at the platinum working electrode and all potentials are refered to $Ag/AgNO_3$ reference electrode. The cyclic voltammograms of *trans*-isomer are shown in figure 34 and *cis*-isomer are shown in figure 35. The results from cyclic voltammetric data show that the isomeric complexes give the similar patterns but the peak potentials are shifted.

In the oxidative potential (positive side) in range +0 to +1.80 V at scan rate 50 mV/s in acetonitrile, has three reversible couples. The two couples are assigned to ligand characters and one couple belongs to the redox of Ru(II/III) couple.

In the reduction potential (negative side), the $Ru(L)_2Cl_2$ displays several peaks in the range –0.20 to –1.80 V at scan rate 50 mV/s. It has one quasi-reversible couple in the range –0.97 to –1.06 V. It is believed that the reduction couple corresponds to the reduction of the azo function. In addition, the result from this range shows one cathodic peak. This occurs in *cis*-isomer but two cathodic peaks are observed in *trans*-isomer. These peaks are the reduced species which are not stable.

Table 36 The cyclic voltammetric data of *trans*- and *cis*-$Ru(L)_2Cl_2$ (L = dmsazpy and desazpy) in 0.1 M TBAH CH_3CN at scan rate 50 mV/s compared with *trans*- and *cis*-$Ru(azpy)_2Cl_2$ (ferrocene used as an internal standard, ΔE = 54 mV)

Compound	$E_{1/2}$, V (ΔE, mV)	
	Oxidation	Reduction
trans-$Ru(dmsazpy)_2Cl_2$	I → +0.27(34) Ru(II/III) → **+0.84(72)** II → +1.02[a]	-0.98(54) -1.25[b] -1.44[b]
trans-$Ru(desazpy)_2Cl_2$	I → +0.24(30) Ru(II/III) → **+0.85(44)** II → +1.02[a]	-1.00(54) -1.28[b] -1.49[b]
trans-$Ru(azpy)_2Cl_2$	Ru(II/III) → **+0.55(60)**	-1.03(50) -1.63(80)
cis-$Ru(dmsazpy)_2Cl_2$	I → +0.38(34) Ru(II/III) → **+0.82(60)** II → +1.07[a]	-1.02(44) -1.37[b]
cis-$Ru(desazpy)_2Cl_2$	I → +0.43(50) Ru(II/III) → **+0.79(98)** II → +1.14[a]	-1.05(50) -1.22[b]
cis-$Ru(azpy)_2Cl_2$	Ru(II/III) → **+0.73(63)**	-0.94(64) -1.77(86)

oxidation potential

The couple I in those complexes are similar to free ligand which occurred spontaneously when scan in the range +0.10 to +0.70 V (figure 40 Appendix C). This couple was quasi-reversible couple. The current increased when higher scan rate was applied. It was one electron transfer process compared with ferrocene couple.

The Ru(II/III) couple was quasi-reversible in the potential range of +0.70 to +1.10 V (Figure 36). It can dividually occur and transfer of one electron.

The couple II was quasi-reversible of ligand because it showed the character similar to those of ligand couple II. It can not spontaneously occur in the ranges +1.10 to +1.30 V. It shows as shoulder at high scan rate (500, 1000, 2000 mV/s) as shown in figure 41 Appendix C.

Reduction potential

All of complexes have more complicated peaks in the range 0 to –1.80 V at scan rate 50 mV/s. There are three cathodic peaks and one anodic peak for those of *trans*-$Ru(L)_2Cl_2$ complexes but the *cis*-$Ru(L)_2Cl_2$complexes show two cathodic and one anodic peaks. However, it has one reversible couple in the range -0.70 to -1.40 V which are adjacent potentials to couples of free ligangs (figure 42 Appendix C). Thus, it can confirm that reductive couple is from the free ligand . The other peaks, which is one cathodic and the other is anodic peak may result from chemically exchange of azo function.

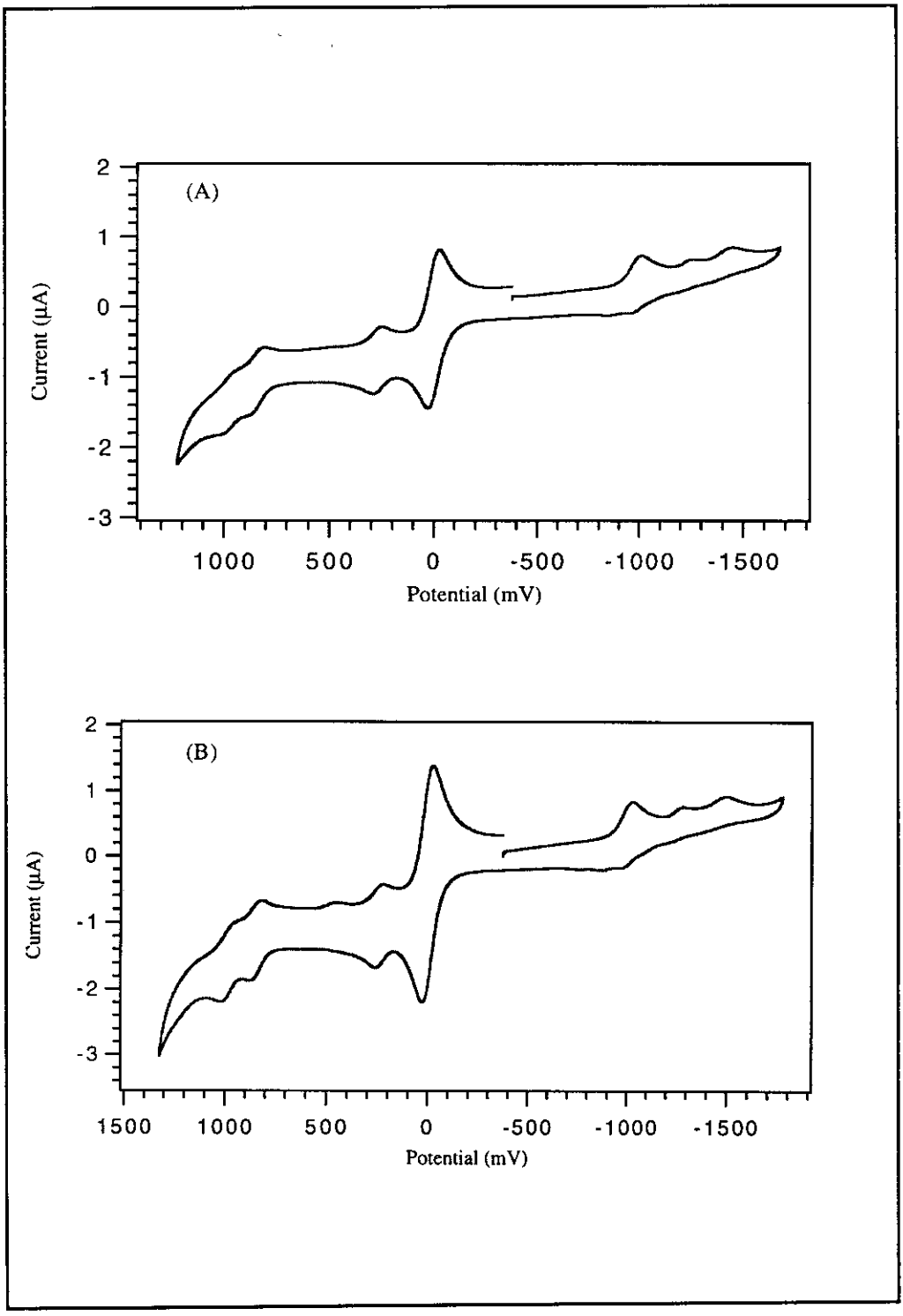

Figure 34 Cyclic voltammograms of (A) *trans*-$Ru(dmsazpy)_2Cl_2$ and (B) *trans*-$Ru(desazpy)_2Cl_2$ in 0.1 M TBAH CH_3CN at scan rate 50 mV/s

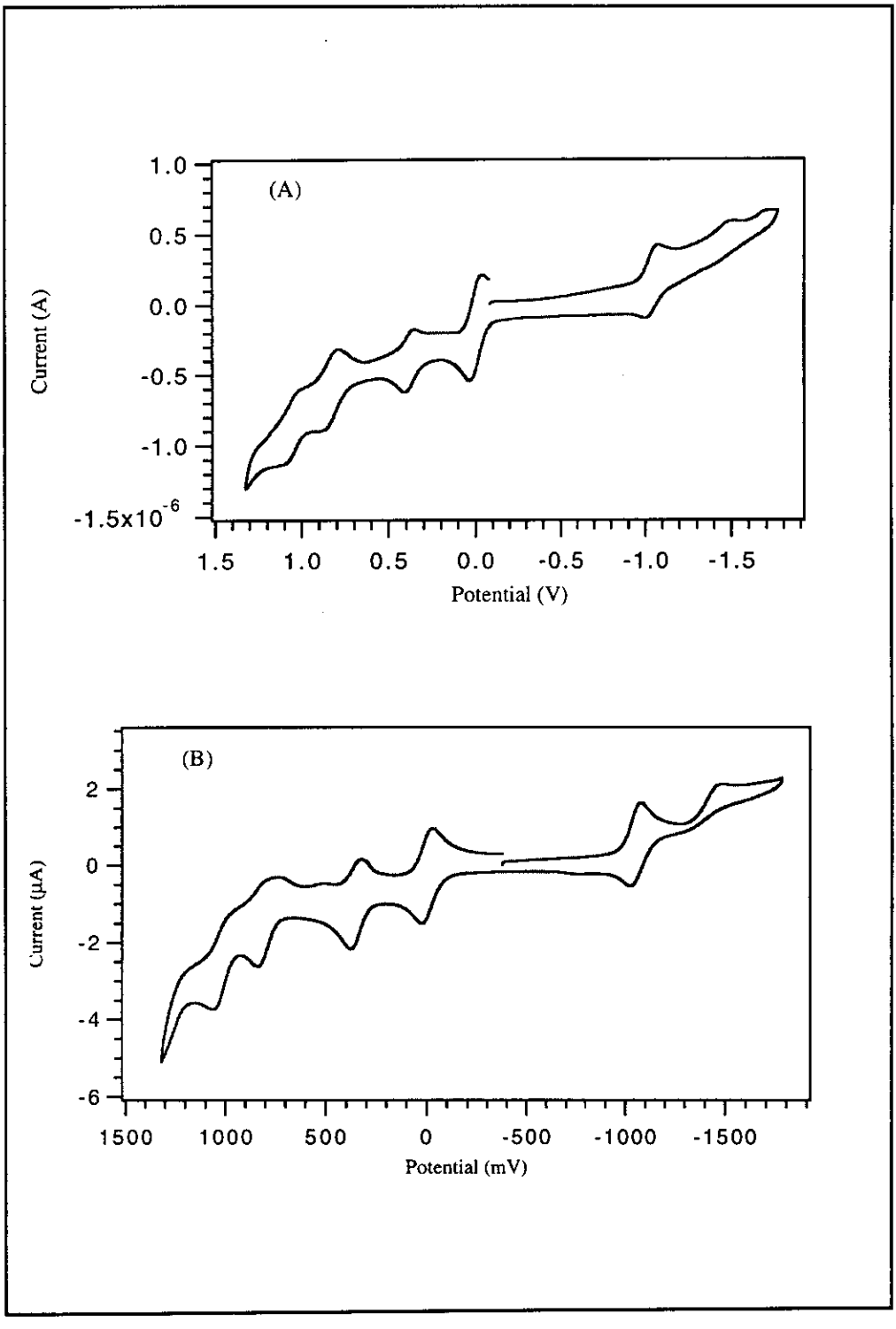

Figure 35 Cyclic voltammograms of (A) *cis*-Ru(dmsazpy)$_2$Cl$_2$ and (B) *cis*-Ru(desazpy)$_2$Cl$_2$ in 0.1 M TBAH CH_3CN at scan rate 50 mV/s

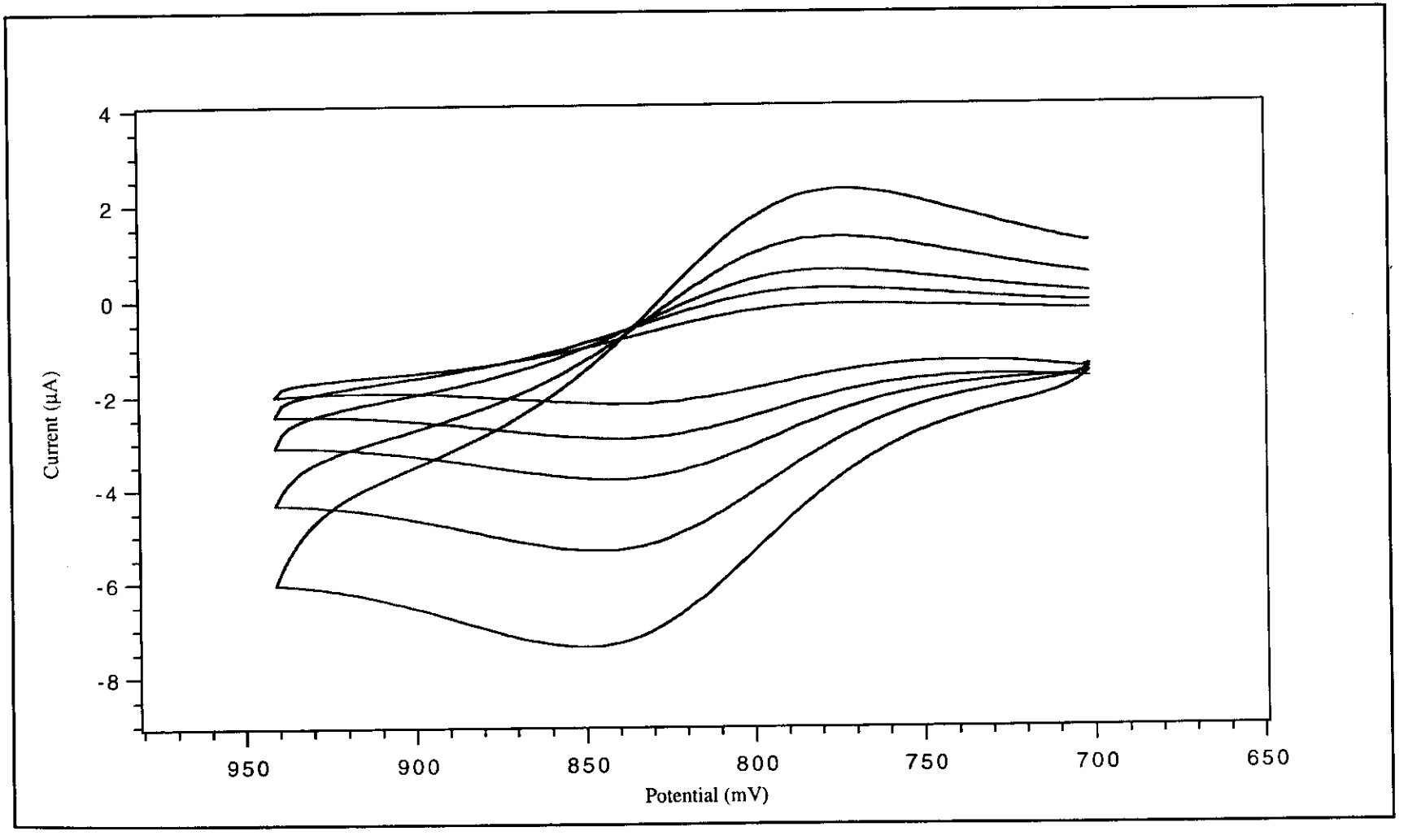

Figure 36 Cyclic voltammograms of quasi-reversible couples of Ru(II/III) scanned with various scan rates (50, 100, 200, 500, 1000 mV/s)